Nuclear Science and Techniques (2025) 36:69
https://doi.org/10.1007/s41365-024-01610-2

Laser-assisted α decay of the deformed odd-*A* nuclei

Jun-Hao Cheng[1] · Qiong Xiao[1] · Jun-Gang Deng[2] · Yang-Yang Xu[1] · You-Tian Zou[1] · Tong-Pu Yu[1]

Received: 3 June 2024 / Revised: 11 September 2024 / Accepted: 19 September 2024 / Published online: 8 March 2025

Abstract
In this study, we explore the impact of state-of-the-art laser fields on the α decay half-life of deformed ground-state odd-*A* nuclei within the proton number range of 52–107. The calculations show that the presence of a laser field modulates the α decay half-life by altering the α decay penetration probability within a limited range. Moreover, the variance in the penetration probability rate of change between even–odd and odd–even nuclei is investigated. Furthermore, we investigate the rate of change of the penetration probability for the same parent nucleus with different neutron numbers, based on the characteristics of the odd-*A* nucleus. We found that the influence of the laser field on the penetration probability is determined by both the shell effect and odd–even staggering. This research contributes to the understanding of nuanced interactions between laser fields and nuclear decay processes. Therefore, valuable insights for future experiments in laser–nuclear physics are attainable using this study.

Keywords α decay · Odd-*A* nuclei · Half-life · Extreme laser field · Penetration probability

1 Introduction

Over the past two decades, the advent of radioactive ion beam facilities worldwide, including those in Dubna, Rikagaku Kenkyusho (RIKEN), Heavy Ion Research Facility in Lanzhou (HIRFL), Berkeley, GSI, and Grand Accelerateur National d'Ions Lourds (GANIL), has spearheaded the discovery of numerous decay modes and exotic nuclei [1–7]. As one of the main decay modes of superheavy nuclei, α decay has attracted considerable attention in the synthesis and research on superheavy nuclei [8–12]. Theoretically, α decay is one of the early successes in quantum mechanics. Gamow [13] and Condon and Gurney [14] independently used the barrier tunneling theory based on quantum mechanics to calculate α decay lifetimes. Experimentally, α decay spectra of neutron-deficient nuclei and heavy and superheavy nuclei provide important nuclear structural information, which makes them irreplaceable for researchers to understand the structure and stability of heavy and superheavy nuclei [15]. The study of α decay processes is paramount for addressing critical challenges, such as deciphering the nuclear cluster structure within superheavy nuclei [16–20], investigating the chronology of the solar system [21], and finding stable superheavy element islands [2].

Laser–nuclear interactions have become a popular topic in nuclear physics research because of their rapidly increasing laser energy and peak intensity. In laboratories, the peak intensity of the produced laser has reached an impressive level of 10^{23} W/cm^2 [22]. In addition, the Extreme Light Infrastructure for Nuclear Physics (ELI-NP) [23, 24] and the Shanghai Superintense Ultrafast Laser Facility (SULF) [25, 26] are expected to further increase the peak laser intensity by one or two orders of magnitude from the current level. These developments provide the basis for a wider range of laser applications [27–29] and the ideal conditions for laser–nuclear interaction studies. Experimentally, Feng *et al.* presented the femtosecond pumping of isomeric nuclear states by the Coulomb excitation of ions with quivering electrons induced by laser fields [30]. Moreover, Shvyd'ko *et al.* used the resonant X-ray excitation of the ^{45}Sc isomer using an X-ray free electron laser [31].

This work was supported by the National Natural Science Foundation of China (Nos. 12375244 and 12135009) and the Hunan Provincial Innovation Foundation for Postgraduate (Nos. CX20210007 and CX20230008).

✉ Tong-Pu Yu
tongpu@nudt.edu.cn

[1] Department of Physics, National University of Defense Technology, Changsha 410073, China

[2] College of Science, China Three Gorges University, Yichang 443002, China

They determined the transition energy with an uncertainty two orders of magnitude smaller. Numerous theoretical studies have focused on the effect of lasers on the decay or fusion of nuclei [23, 32–38]. However, it is worth noting that most such investigations have predominantly centered on the influence of lasers on even–even nuclei. The effect of laser fields on the half-life of odd-*A* nuclei is yet to be extensively explored.

Recently, we performed quantitative calculations of the α -decay half-life of laser-affected even–even nuclei based on the semi-classical Wentzel–Kramers–Brillouin (WKB) approximation [39]. Our current work expands this to determine the effect of lasers on the α-decay half-life of odd-*A* nuclei. To accurately calculate the laser–nucleus interaction, the deformation of the nuclei must be considered because the introduced electric dipole term is closely related to the vector angle between $E(t)$ and r. We systematically analyzed the rate of change in the α-decay half-life of deformed ground-state odd-*A* nuclei with a proton number of $52 \leq Z \leq 107$ using a state-of-the-art laser pulse. The Coulomb potential was calculated using a double-folding model, and the nuclear potential was calculated using the deformed Woods–Saxon nuclear potential [40]. Our findings indicate that ^{151}Eu is the odd-*A* parent nucleus most sensitive to intense laser pulses. Moreover, we discuss in detail the influence of the shell effect and odd–even staggering of the odd-*A* nucleus on the rate of change in the α -decay penetration probability.

The remainder of this paper is organized as follows. In the next section, the theoretical framework for calculating the α -decay half-life in ultraintense laser fields is described in detail. Detailed calculation results and discussion are provided in Sect. 3. Section 4 provides the summary.

2 Theoretical framework

2.1 The theoretical method

α-decay half-life $T_{1/2}$, which is an important indicator of nuclear stability, can be expressed as follows:

$$T_{1/2} = \frac{\hbar \ln 2}{\Gamma}, \tag{1}$$

where $\hbar$ denotes reduced Planck's constant. Γ denotes the α -decay width, which can be written as follows [41]:

$$\Gamma = \frac{\hbar^2}{4\mu} S_\alpha F P, \tag{2}$$

where S_α, F, and P are the α-particle formation probability, normalized factor, and penetration probability, respectively. $\mu = \frac{M_d M_\alpha}{M_d + M_\alpha}$ is the reduced mass of the α particles and daughter nuclei in center-of-mass coordinates. Here, M_d and M_α are the masses of the daughter nucleus and α particle, respectively.

Considering the impact of nucleus deformation, the total penetration probability P is determined by averaging P_φ across all the orientations. This methodology is frequently employed to compute α decay and fusion reactions [42–46] and is succinctly expressed as follows [47]:

$$P = \frac{1}{2} \int_0^\pi P_\varphi \sin\varphi \mathrm{d}\varphi, \tag{3}$$

$$P_\varphi = \exp\left[-2 \int_{R_2}^{R_3} k(r, t, \varphi, \theta)\, \mathrm{d}r\right], \tag{4}$$

where r denotes the separation between the mass center of α particle and the mass center of the core. The variable φ denotes the orientation angle of the symmetry axis of the daughter nucleus relative to the emitted α particle. θ is related to the interaction between the laser and the nucleus, which is explained in more detail in the following subsection. The classical turning points, denoted by R_1, R_2, and R_3, can be calculated using the equation $V(r, t, \varphi, \theta) = Q_\alpha$. The wavenumber, represented by $k(r, t, \varphi, \theta)$, can be expressed as follows:

$$k(r, t, \varphi, \theta) = \sqrt{\frac{2\mu}{\hbar^2} \mid V(r, t, \varphi, \theta) - Q_\alpha \mid}, \tag{5}$$

where Q_α denotes the α decay energy. Similarly, the normalized factor F can be obtained as follows:

$$F = \frac{1}{2} \int_0^\pi F_\varphi \sin\varphi \mathrm{d}\varphi, \tag{6}$$

$$F_\varphi = \frac{1}{\int_{R_1}^{R_2} \frac{1}{2k(r,t,\varphi,\theta)}\, \mathrm{d}r}. \tag{7}$$

In this study, the total interaction potential $V(r, t, \varphi, \theta)$ between the daughter nucleus and emitted α particles can be expressed as follows:

$$V(r, t, \varphi, \theta) = \lambda(\varphi) V_\mathrm{N}(r, \varphi) + V_\mathrm{l}(r) + V_\mathrm{C}(r, \varphi) + V_\mathrm{i}(r, t, \varphi, \theta), \tag{8}$$

where $V_\mathrm{l}(r)$, $V_\mathrm{C}(r, \varphi)$, and $V_\mathrm{N}(r, \varphi)$ are the centrifugal, Coulomb, and nuclear potentials, respectively. The interaction between the electromagnetic field and decay system is described by $V_\mathrm{i}(r, t, \varphi, \theta)$ [48], and a detailed explanation of this interaction is provided in the subsequent subsection. The value of $\lambda(\varphi)$ can be determined using the Bohr–Sommerfeld quantization condition.

The deformed Coulomb potential is obtained using the double-folding mode, which is given by [47]

$$V_{\mathrm{C}}(\vec{r},\varphi)=\int\int\frac{\rho_{\mathrm{d}}(\vec{r}_{\mathrm{d}})\rho_{\alpha}(\vec{r}_{\alpha})}{\mid\vec{r}+\vec{r}_{\mathrm{d}}-\vec{r}_{\alpha}\mid}\mathrm{d}\vec{r}_{\alpha}\mathrm{d}\vec{r}_{\mathrm{d}},\tag{9}$$

where $\vec{r}_{\mathrm{d}}$ and $\vec{r}_{\alpha}$ represent the radius vectors in the charge distributions of daughter nuclei and emitted α particle, respectively. ρ_{d} and ρ_{α} represent the density distributions of the daughter nucleus and emitted α particle, respectively. This approximation is simplified using an appropriate Fourier transform, as demonstrated in Ref. [49–51]. The Coulomb potential can be approximated as follows:

$$V_{\mathrm{C}}(\vec{r},\varphi)=V_{\mathrm{C}}^{(0)}(\vec{r},\varphi)+V_{\mathrm{C}}^{(1)}(\vec{r},\varphi)+V_{\mathrm{C}}^{(2)}(\vec{r},\varphi),\tag{10}$$

where $V_{\mathrm{C}}^{(0)}(\vec{r},\varphi)$, $V_{\mathrm{C}}^{(1)}(\vec{r},\varphi)$, and $V_{\mathrm{C}}^{(2)}(\vec{r},\varphi)$ are the bare Coulomb interaction, linear Coulomb coupling, and second-order Coulomb coupling, respectively [49]. The Langer-modified $V_{\mathrm{l}}(r)$ is selected in the form [52], which is given by the following equation:

$$V_{\mathrm{l}}(r)=\frac{\hbar^2(l+\frac{1}{2})^2}{2\mu r^2},\tag{11}$$

where l denotes the orbital angular momentum of the α particle.

In this study, the emitted α-daughter nucleus nuclear potential $V_{\mathrm{N}}(r,\varphi)$ is selected as the classical Woods–Saxon (WS) nuclear potential [40], which is expressed as follows:

$$V_{\mathrm{N}}(r,\varphi)=\frac{V'}{1+\exp[(r-R_{\mathrm{d}}(\varphi))/s]}.\tag{12}$$

Changing the radius in the Woods–Saxon potential to a dynamic operator yields the nuclear coupling component [53, 54]. In addition, $R_{\mathrm{d}}(\varphi)$ can be written as follows:

$$R_{\mathrm{d}}(\varphi)=r_0A_{\mathrm{d}}^{1/3}[1+\beta_2Y_{20}(\varphi)+\beta_4Y_{40}(\varphi)+\beta_6Y_{60}(\varphi)].\tag{13}$$

The ground-state nuclear deformations are denoted by β_2, β_4, and β_6, which represent the quadrupole, hexadecapole, and hexacontatetrapole deformations, respectively. A_{d} denotes the mass of the daughter nucleus. $Y_{\mathrm{ml}}(\varphi)$ is a spherical harmonic function, r_0, s, and V' are the adjustable parameter radii, diffuseness, and depth of the nuclear potential, respectively.

2.2 Laser–nucleus interaction

2.2.1 Quasistatic approximation

The full width at half maximum (FWHM) of laser pulses with peak intensities exceeding 10^{23} W/cm^2 currently available in the laboratory is approximately 19.6 fs ($=1.96\times10^{-14}$ s) [22]. The laser cycles produced by a near-infrared laser with a wavelength of approximately 800 nm and an X-ray free electron laser [56] with a photon energy of 10 keV are approximately 10^{-15} s and 10^{-19} s, respectively. For α decay, the emitted α particles oscillate back and forth at high frequencies within the parent nuclei, with a small probability of tunneling out whenever the preformed α particles hit the potential wall. Because the typical decay energy for α decay is approximately several MeV, the velocity of the preformed α particles is approximately 10^7 m/s. In addition, the size of the parent nucleus is approximately 1 fm, and the frequency of the oscillations can be roughly estimated to be 10^{22} Hz. The length of the tunnel path is less than 100 fm, and the time for the emitted α particles to pass through the tunnel is less than 10^{-20} s. From a quantum mechanical perspective, the collision frequency ν of the emitted α particles can be calculated using the oscillation frequency as follows: [57]

$$\nu=\Omega/2\pi=\frac{(2n_r+l+\frac{3}{2})\hbar}{2\pi\mu{R_{\mathrm{n}}}^2}=\frac{(G+\frac{3}{2})\hbar}{1.2\pi\mu{R_0}^2},\tag{14}$$

where R_{n} denotes the root-mean-square radius of the nucleus. $G=2n_{\mathrm{r}}+l$ denotes the main quantum number [58], where l and n_{r} are the angular and radial quantum numbers of the emitted particles, respectively. The calculations indicate that the typical collision frequency of α particles is greater than 10^{21} Hz. The highest peak intensity laser pulse currently achievable has an optical period that is much longer than this. Therefore, the laser field does not change significantly during the passage of the emitted α particles through the potential barrier, and the process can be considered quasi-static. A similar quasi-static approximation is typically used to describe the tunneling ionization of atoms in strong field atomic physics [59, 60].

Finally, the kinetic energy of the emitted α particles is only a few MeV. They move much slower than light in vacuum. This implies that the effect of the laser electric field on the emitted α particles is significantly larger than that of the laser magnetic field. Therefore, the magnetic component of the laser field is neglected in this study.

2.2.2 Relative motion of daughter nuclei and α particles in laser fields in center-of-mass coordinates

In the framework of the quasi-static approximation, the interaction between the daughter nucleus and emitted α particle can be effectively described using the time-dependent Schrödinger equation (TDSE) [61], which can be expressed as follows:

$$i\hbar\frac{\partial\Phi(\vec{r}_{\alpha},\vec{r}_{\mathrm{d}},t)}{\partial t}=H(t)\Phi(\vec{r}_{\alpha},\vec{r}_{\mathrm{d}},t),\tag{15}$$

where $H(t)$ represents the time-dependent minimum-coupling Hamiltonian, which can be written as follows:

$$H(t) = \sum_i \frac{1}{2m_i}\left[\vec{p}_i - \frac{q_i}{c}\vec{A}(t)\right]^2 + V(r), \tag{16}$$

where i is a parameter related to the daughter nucleus and the emitted α particle.

For the center-of-mass coordinates $(\vec{R}, \vec{P}, \vec{r}, \vec{p})$,

$$\begin{aligned}
\vec{r}_\alpha &= \vec{R} + m_\mathrm{d}\vec{r}/(m_\alpha + m_\mathrm{d}) \\
\vec{p}_\alpha &= \vec{p} + m_\alpha\vec{P}/(m_\alpha + m_\mathrm{d}) \\
\vec{r}_\mathrm{d} &= \vec{R} - m_\alpha\vec{r}/(m_\alpha + m_\mathrm{d}) \\
\vec{p}_\mathrm{d} &= -\vec{p} + m_\mathrm{d}\vec{P}/(m_\alpha + m_\mathrm{d}).
\end{aligned} \tag{17}$$

The time-dependent minimum-coupling Hamiltonian is obtained as follows:

$$H(t) = \frac{1}{2M}\left[\vec{P} - \frac{q}{c}\vec{A}(t)\right]^2 + \frac{1}{2\mu}\left[\vec{p} - \frac{Q_\mathrm{eff}}{c}\vec{A}(t)\right]^2 + V(r), \tag{18}$$

where $q = q_\alpha + q_\mathrm{d}$ and $M = m_\alpha + m_\mathrm{d}$. Q_eff represents the effective charge for relative motion, which describes the tendency of the laser electric field to separate the emitted α particles from the daughter nuclei. It can be obtained as follows:

$$Q_\mathrm{eff} = \frac{q_\alpha m_\mathrm{d} - q_\mathrm{d} m_\alpha}{M}. \tag{19}$$

By introducing unitary transformations, the wave function can be transformed into center-of-mass coordinates as follows:

$$\phi(\vec{r}, \vec{R}, t) = \hat{U}_r\hat{U}_R\Phi(\vec{r}, \vec{R}, t), \tag{20}$$

where $\hat{U}_r = \exp\left[-i\frac{Q_\mathrm{eff}}{c}\vec{A}(t)\cdot\vec{r}/\hbar\right]$ and $\hat{U}_R = \exp\left[-i\frac{q}{c}\vec{A}(t)\cdot\vec{R}/\hbar\right]$. The TDSE can be rewritten as follows:

$$\begin{aligned}
i\hbar\frac{\partial\phi(\vec{r}, \vec{R}, t)}{\partial t} = &\left[-\frac{\hbar^2}{2\mu}\nabla_r^2 + V(r) - Q_\mathrm{eff}\vec{r}\vec{E}(t)\right. \\
&\left.-\frac{\hbar^2}{2M}\nabla_R^2 - q\vec{R}\vec{E}(t)\right]\phi(\vec{r}, \vec{R}, t),
\end{aligned} \tag{21}$$

where $c\vec{E}(t) = -\mathrm{d}\vec{A}(t)/\mathrm{d}t$ denotes the time-dependent laser electric field. For simplicity, we factorize the wavefunction $\phi(\vec{r}, \vec{R}, t)$ into two parts: $\phi(\vec{r}, \vec{R}, t) = \chi_1(\vec{R}, t)\chi_2(\vec{r}, t)$. This allows us to split the TDSE into two separate equations that describe the center-of-mass coordinates and the relative motion between the daughter nucleus and the emitted α particle. The two equations can be written as follows:

$$i\hbar\frac{\partial\chi_1(\vec{R}, t)}{\partial t} = \left[-\frac{\hbar^2}{2M}\nabla_R^2 - q\vec{R}\vec{E}(t)\right]\chi_1(\vec{R}, t), \tag{22}$$

$$i\hbar\frac{\partial\chi_2(\vec{r}, t)}{\partial t} = \left[-\frac{\hbar^2}{2\mu}\nabla_r^2 + V(r) - Q_\mathrm{eff}\vec{r}\vec{E}(t)\right]\chi_2(\vec{r}, t). \tag{23}$$

The equation describing the relative motion is intricately linked to the electric field produced by the laser. This connection allows for the formulation of the interaction potential energy, which characterizes the interactions between a particle undergoing relative motion and the laser field. In addition, the connection can be obtained as follows:

$$V_i(\vec{r}, t, \theta) = -Q_\mathrm{eff}\vec{r}\cdot\vec{E}(t) = -Q_\mathrm{eff}rE(t)\cos\theta, \tag{24}$$

where θ denotes the angle between vectors $\vec{r}$ and $\vec{E}(t)$.

2.2.3 Laser–nucleus interaction

The real laser electric field should be represented as a linearly polarized Gaussian plane waveform, which can be written as follows:

$$E(t) = E_0 f(t)\sin(\omega t), \tag{25}$$

where ω denotes angular frequency. The peak of the laser electric field is $E_0[\mathrm{V\ cm^{-1}}]=27.44(I_0[\mathrm{W\ cm^{-2}}])^{1/2}$ and I_0 is the peak laser intensity [23]. $f(t)$ is a sequence of Gaussian pulses with an envelope function of the temporal profile, which can be expressed as follows:

$$f(t) = \exp\left(-\frac{t^2}{\tau^2}\right). \tag{26}$$

The pulse width of the envelope τ can be expressed in terms of pulse period T_0 as follows:

$$\tau = xT_0. \tag{27}$$

Combined with the expression for the electric field, $E(t)$ can be written in a wavelength-dependent form as follows:

$$\begin{aligned}
E(t) &= E_0\exp\left(-\frac{t^2}{x^2T_0^2}\right)\sin(\omega t) \\
&= E_0\exp\left(-\frac{c^2t^2}{\lambda^2x^2}\right)\sin\left(2\pi\frac{c}{\lambda}t\right),
\end{aligned} \tag{28}$$

where λ denotes laser wavelength. The pulse period is $T_0 = 1/\nu$, and $\nu = \omega/2\pi = c/\lambda$ is the laser frequency.

In the context of the interaction between laser electric fields and nuclear processes, it is pertinent to consider the influence of laser electric fields on the decay energy Q_α. The alteration in the decay energy ΔQ_α is equivalent to the energy of the α particle accelerated by the laser electric field while it penetrates the potential barrier. Therefore, the alteration can be expressed as follows:

$$\Delta Q_\alpha = eZ_\alpha E(t) R_d(\varphi)\cos\theta. \tag{29}$$

The α decay energy, considering the laser electric field effect Q^*_α, can thus be rewritten as follows:

$$Q^*_\alpha = Q_\alpha + \Delta Q_\alpha. \tag{30}$$

3 Results and discussion

In this study, the least-squares principle was used to refit the adjustable parameters within the WS nuclear potential. S_α was approximated to be 0.35 based on Ref. [55], whereas the deformation parameters β_2, β_4, and β_6 utilized for the fitting process were obtained from FRDM2012 [62]. To ensure accuracy, experimental data on α decay energy Q_α, spin, parity, and α decay half-lives were gathered from the latest evaluated atomic mass table AME2020 [63, 64] and the latest evaluated nuclear properties table NUBASE2020 [65]. The standard deviation σ, representing the difference between theoretical and experimental α decay half-lives, is calculated as $\sigma = \sqrt{\sum\left(\lg T^{exp}_{1/2}(s) - \lg T^{cal}_{1/2}(s)\right)^2/n}$. The theoretical α-decay half-lives were obtained by integration using Eqs. (2)-(7). The adjustable parameters are determined without considering the laser field, resulting in an optimal standard deviation of $\sigma = 0.600$. The most convenient values for the attenuation calculation are given by:

$$r_0 = 1.10\ \text{fm}, s = 0.92\ \text{fm}, V' = 173.64\ \text{MeV}. \tag{31}$$

Table 1 presents the comprehensive results obtained in this study. The initial five columns show the parent nuclei, decay energy Q_α, orbital angular momentum l, and logarithmic forms of both the experimental and theoretical α-decay half-lives. As shown in this table, for the vast majority of parent nuclei, the theoretical half-life of α decay obtained by our model is in good agreement with the experimental data. Furthermore, the most laser sensitive in the odd-A nucleus (^{151}Eu) exhibited almost the same decay energy and δP as the most laser-sensitive nucleus in the even–even nucleus (^{144}Nd) in the case of $I = 10^{23}$ W/cm^2 [39].

To provide a more intuitive comparison of the theoretical half-life of α decay with experimental data, Fig. 1a meticulously displays both the experimental data (T^{exp}) and the corresponding theoretical half-life values (T^{cal}) of odd-A nuclear α decay. The congruence between the calculations and experimental outcomes for most nuclei half-lives is pronounced, as shown in the figure. Moreover, Fig. 1b shows the disparities between the calculations concerning α-decay half-lives of various parent nuclei and their corresponding experimental findings. It was observed that the absolute deviation values between the experimental data and calculations were within 1 for most parent nuclei, indicating an agreement between the theoretical half-lives of α decay and the experimental data. Moreover, this indicates that the model we used was reliable.

Based on Eq. (8) and (30), the laser electric field affects the nucleus' α decay penetration probability. This impact is owing to the alteration of the total potential barrier height and the energy of the α particle, which ultimately affects the α-decay half-life. In this study, we define the effect of the laser electric field on the nucleus α-decay penetration probability as the rate of change in the penetration probability δP, which is as follows:

$$\delta P = \frac{P(E) - P(E=0)}{P(E=0)}. \tag{32}$$

The normalized factor F, delineated by the principal quantum number G [66], exhibits negligible responsiveness to the external laser field, which is attributable to the integration occurring within the nucleus from R_1 to R_2. Consequently, it is reasonable to consider the normalization factor F as a constant independent of the laser [61]. Therefore, we suggested that the primary influence of the external laser fields on the half-life of α decay occurs through alterations in the probability of α-decay penetration. According to Eq. (1) and (2), we can define the effect of the laser electric field on the nucleus α-decay half-life as the rate of change of the half-life δT, which is obtained as follows:

$$\delta T = \frac{T(E) - T(E=0)}{T(E=0)} = \frac{P(E=0) - P(E)}{P(E)}. \tag{33}$$

The last four columns in Table 1 show the rate of change of the penetration probability and half-life of the ground-state odd-A nucleus for laser intensities of $I = 10^{23}$ W/cm^2 and $I = 10^{24}$ W/cm^2, respectively. When the laser electric field was aligned ($\cos\theta = 1$) with the α particle emission direction, it was observed that for most parent nuclei, laser intensities of $I = 10^{23}$ W/cm^2 and $I = 10^{24}$ W/cm^2 lead to slight changes to both the α-decay penetration probability and half-life. Moreover, the nucleus ^{151}Eu exhibited the highest sensitivity to the laser electric field and showed a change in the α-decay penetration probability of 1.386‰and 4.388‰ for laser intensities of $I = 10^{23}$ W/cm^2 and $I = 10^{24}$ W/cm^2, respectively.

To better show the impact of the laser electric field on the α decay of odd-A nuclei, we illustrated δP from Table 1 in Fig. 2. It is worth noting that the absolute values of the rate of change of the half-life and penetration probability were nearly identical for the laser intensities of $I = 10^{23}$ W/cm^2 and $I = 10^{24}$ W/cm^2. Therefore, our subsequent analysis concentrates solely on the rate of change in the penetration probability. In this study, we classified the odd-A nuclei into two categories based on

Table 1 Comparison of experimental and calculated α -decay half-lives and the impact of laser field with intensities of 10^{23} W/cm^2 and 10^{24} W/cm^2 on ground-state odd-A nuclei

Nucleus	Q_α (MeV)	l	lg$T_{\rm exp}$ (s)	lg$T_{\rm cal}$ (s)	δP^{23}	δT^{23}	δP^{24}	δT^{24}
^{105}Te	5.069	0	−6.199	−7.582	8.400×10^{-5}	-8.400×10^{-5}	2.700×10^{-4}	-2.700×10^{-4}
^{109}Te	3.198	0	2.051	1.789	2.171×10^{-4}	-2.171×10^{-4}	6.871×10^{-4}	-6.866×10^{-4}
^{109}I	3.918	2	−0.191	−1.648	1.426×10^{-4}	-1.426×10^{-4}	4.571×10^{-4}	-4.569×10^{-4}
^{113}I	2.707	0	7.300	6.582	3.295×10^{-4}	-3.294×10^{-4}	1.048×10^{-3}	-1.047×10^{-3}
^{109}Xe	4.217	0	−1.886	−2.961	1.205×10^{-4}	-1.204×10^{-4}	3.804×10^{-4}	-3.802×10^{-4}
^{145}Pm	2.322	0	17.300	17.266	8.836×10^{-4}	-8.828×10^{-4}	2.790×10^{-3}	-2.782×10^{-3}
^{147}Sm	2.311	0	18.527	18.259	9.104×10^{-4}	-9.096×10^{-4}	2.876×10^{-3}	-2.868×10^{-3}
^{147}Eu	2.991	0	10.964	11.055	5.188×10^{-4}	-5.185×10^{-4}	1.644×10^{-3}	-1.642×10^{-3}
^{151}Eu	1.964	2	26.162	25.173	1.386×10^{-3}	-1.384×10^{-3}	4.388×10^{-3}	-4.369×10^{-3}
^{149}Gd	3.099	0	11.271	10.739	4.913×10^{-4}	-4.911×10^{-4}	1.558×10^{-3}	-1.556×10^{-3}
^{151}Gd	2.652	0	14.988	15.477	7.127×10^{-4}	-7.122×10^{-4}	2.260×10^{-3}	-2.255×10^{-3}
^{149}Tb	4.078	2	4.948	4.197	2.820×10^{-4}	-2.819×10^{-4}	8.932×10^{-4}	-8.924×10^{-4}
^{151}Tb	3.496	2	8.824	8.329	3.974×10^{-4}	-3.972×10^{-4}	1.256×10^{-3}	-1.255×10^{-3}
^{151}Dy	4.180	0	4.280	3.826	2.718×10^{-4}	-2.717×10^{-4}	8.622×10^{-4}	-8.615×10^{-4}
^{153}Dy	3.559	0	8.389	8.143	3.902×10^{-4}	-3.900×10^{-4}	1.237×10^{-3}	-1.236×10^{-3}
^{151}Ho	4.695	0	2.198	1.479	2.137×10^{-4}	-2.136×10^{-4}	6.776×10^{-4}	-6.772×10^{-4}
^{153}Ho	4.052	0	5.372	5.252	2.909×10^{-4}	-2.908×10^{-4}	9.314×10^{-4}	-9.305×10^{-4}
^{153}Er	4.802	0	1.843	1.467	2.075×10^{-4}	-2.074×10^{-4}	6.604×10^{-4}	-6.600×10^{-4}
^{155}Er	4.118	0	6.146	5.419	2.970×10^{-4}	-2.969×10^{-4}	9.266×10^{-4}	-9.257×10^{-4}
^{155}Tm	4.572	0	3.414	3.270	2.350×10^{-4}	-2.349×10^{-4}	7.394×10^{-4}	-7.389×10^{-4}
^{157}Tm	3.878	5	7.463	9.340	3.426×10^{-4}	-3.425×10^{-4}	1.082×10^{-3}	-1.081×10^{-3}
^{155}Yb	5.339	0	0.302	−0.045	1.680×10^{-4}	-1.679×10^{-4}	5.383×10^{-4}	-5.381×10^{-4}
^{155}Lu	5.802	0	−1.123	−1.513	1.454×10^{-4}	-1.453×10^{-4}	4.549×10^{-4}	-4.547×10^{-4}
^{157}Hf	5.880	0	−0.914	−1.345	1.413×10^{-4}	-1.413×10^{-4}	4.519×10^{-4}	-4.517×10^{-4}
^{159}Hf	5.225	0	1.163	1.510	1.863×10^{-4}	-1.863×10^{-4}	5.872×10^{-4}	-5.869×10^{-4}
^{157}Ta	6.355	5	−1.981	−1.140	1.239×10^{-4}	-1.239×10^{-4}	3.902×10^{-4}	-3.901×10^{-4}
^{159}Ta	5.681	0	0.479	−0.042	1.548×10^{-4}	-1.547×10^{-4}	4.901×10^{-4}	-4.899×10^{-4}
^{161}W	5.923	0	−0.253	−0.571	1.469×10^{-4}	-1.469×10^{-4}	4.654×10^{-4}	-4.652×10^{-4}
^{163}W	5.520	0	1.268	1.142	1.759×10^{-4}	-1.758×10^{-4}	5.532×10^{-4}	-5.529×10^{-4}
^{167}W	4.751	0	4.686	5.043	2.473×10^{-4}	-2.472×10^{-4}	7.866×10^{-4}	-7.860×10^{-4}
^{163}Re	6.012	0	0.082	−0.460	1.469×10^{-4}	-1.468×10^{-4}	4.626×10^{-4}	-4.624×10^{-4}
^{165}Re	5.694	0	1.034	0.862	1.689×10^{-4}	-1.688×10^{-4}	5.327×10^{-4}	-5.324×10^{-4}
^{169}Re	5.014	5	5.184	5.677	2.286×10^{-4}	-2.285×10^{-4}	7.354×10^{-4}	-7.349×10^{-4}
^{161}Os	7.069	0	−3.194	−3.778	1.026×10^{-4}	-1.026×10^{-4}	3.256×10^{-4}	-3.254×10^{-4}
^{167}Os	5.980	0	0.213	0.122	1.555×10^{-4}	-1.555×10^{-4}	4.965×10^{-4}	-4.963×10^{-4}
^{169}Os	5.713	0	1.400	1.251	1.747×10^{-4}	-1.747×10^{-4}	5.553×10^{-4}	-5.550×10^{-4}
^{171}Os	5.371	0	2.663	2.828	2.058×10^{-4}	-2.058×10^{-4}	6.485×10^{-4}	-6.481×10^{-4}
^{173}Os	5.055	0	3.727	4.422	2.386×10^{-4}	-2.386×10^{-4}	7.555×10^{-4}	-7.550×10^{-4}
^{167}Ir	6.505	0	−1.172	−1.446	1.318×10^{-4}	-1.318×10^{-4}	4.166×10^{-4}	-4.164×10^{-4}
^{169}Ir	6.141	0	−0.182	−0.063	1.487×10^{-4}	-1.487×10^{-4}	4.789×10^{-4}	-4.787×10^{-4}
^{171}Ir	5.997	0	1.310	0.510	1.656×10^{-4}	-1.656×10^{-4}	5.201×10^{-4}	-5.199×10^{-4}
^{173}Ir	5.716	3	2.408	2.312	1.858×10^{-4}	-1.858×10^{-4}	5.901×10^{-4}	-5.898×10^{-4}
^{175}Ir	5.430	5	3.023	4.538	2.128×10^{-4}	-2.127×10^{-4}	6.808×10^{-4}	-6.803×10^{-4}
^{177}Ir	5.080	0	4.689	4.802	2.482×10^{-4}	-2.481×10^{-4}	7.881×10^{-4}	-7.875×10^{-4}
^{165}Pt	7.453	0	−3.432	−4.150	9.843×10^{-5}	-9.842×10^{-5}	3.095×10^{-4}	-3.094×10^{-4}
^{171}Pt	6.607	0	−1.278	−1.399	1.336×10^{-4}	-1.335×10^{-4}	4.268×10^{-4}	-4.267×10^{-4}
^{173}Pt	6.360	0	−0.354	−0.493	1.488×10^{-4}	-1.488×10^{-4}	4.749×10^{-4}	-4.746×10^{-4}
^{175}Pt	6.164	2	0.576	0.567	1.629×10^{-4}	-1.629×10^{-4}	5.192×10^{-4}	-5.189×10^{-4}

Table 1 (continued)

Nucleus	Q_α (MeV)	l	lg$T_{\rm exp}$ (s)	lg$T_{\rm cal}$ (s)	δP^{23}	δT^{23}	δP^{24}	δT^{24}
^{177}Pt	5.643	0	2.240	2.512	2.018×10^{-4}	-2.018×10^{-4}	6.318×10^{-4}	-6.314×10^{-4}
^{179}Pt	5.412	2	3.941	3.908	2.284×10^{-4}	-2.283×10^{-4}	7.115×10^{-4}	-7.110×10^{-4}
^{181}Pt	5.150	0	4.847	4.943	2.518×10^{-4}	-2.517×10^{-4}	8.027×10^{-4}	-8.020×10^{-4}
^{183}Pt	4.822	0	6.607	6.776	2.962×10^{-4}	-2.961×10^{-4}	9.413×10^{-4}	-9.404×10^{-4}
^{185}Pt	4.437	5	7.928	10.720	3.660×10^{-4}	-3.659×10^{-4}	1.158×10^{-3}	-1.157×10^{-3}
^{173}Au	6.836	0	−1.529	−1.780	1.295×10^{-4}	-1.295×10^{-4}	4.072×10^{-4}	-4.070×10^{-4}
^{175}Au	6.583	0	−0.645	−0.883	1.430×10^{-4}	-1.430×10^{-4}	4.509×10^{-4}	-4.507×10^{-4}
^{177}Au	6.298	0	0.568	0.191	1.585×10^{-4}	-1.585×10^{-4}	5.058×10^{-4}	-5.055×10^{-4}
^{179}Au	5.981	0	1.507	1.485	1.819×10^{-4}	-1.818×10^{-4}	5.770×10^{-4}	-5.767×10^{-4}
^{181}Au	5.751	0	2.697	2.489	2.041×10^{-4}	-2.041×10^{-4}	6.470×10^{-4}	-6.466×10^{-4}
^{183}Au	5.465	0	3.889	3.834	2.268×10^{-4}	-2.267×10^{-4}	7.272×10^{-4}	-7.267×10^{-4}
^{185}Au	5.180	0	4.982	5.295	2.661×10^{-4}	-2.660×10^{-4}	8.307×10^{-4}	-8.300×10^{-4}
^{175}Hg	7.072	0	−1.991	−2.169	1.227×10^{-4}	-1.227×10^{-4}	3.903×10^{-4}	-3.902×10^{-4}
^{177}Hg	6.740	2	−0.932	−0.726	1.383×10^{-4}	-1.383×10^{-4}	4.426×10^{-4}	-4.424×10^{-4}
^{179}Hg	6.350	0	0.144	0.445	1.613×10^{-4}	-1.613×10^{-4}	5.086×10^{-4}	-5.084×10^{-4}
^{181}Hg	6.284	2	1.122	0.969	1.732×10^{-4}	-1.732×10^{-4}	5.435×10^{-4}	-5.432×10^{-4}
^{183}Hg	6.039	0	1.904	1.692	1.874×10^{-4}	-1.873×10^{-4}	5.962×10^{-4}	-5.959×10^{-4}
^{185}Hg	5.773	0	2.906	2.858	2.125×10^{-4}	-2.125×10^{-4}	6.696×10^{-4}	-6.692×10^{-4}
^{177}Tl	7.067	0	−1.609	−1.722	1.257×10^{-4}	-1.257×10^{-4}	3.968×10^{-4}	-3.967×10^{-4}
^{179}Tl	6.709	0	−0.139	−0.457	1.425×10^{-4}	-1.425×10^{-4}	4.489×10^{-4}	-4.487×10^{-4}
^{181}Tl	6.322	0	1.525	1.030	1.622×10^{-4}	-1.622×10^{-4}	5.178×10^{-4}	-5.175×10^{-4}
^{179}Pb	7.596	2	−2.569	−2.752	1.112×10^{-4}	-1.112×10^{-4}	3.524×10^{-4}	-3.522×10^{-4}
^{181}Pb	7.240	2	−1.409	−1.621	1.255×10^{-4}	-1.255×10^{-4}	3.982×10^{-4}	-3.981×10^{-4}
^{183}Pb	6.928	1	−0.272	−0.755	1.398×10^{-4}	-1.398×10^{-4}	4.449×10^{-4}	-4.447×10^{-4}
^{185}Pb	6.695	2	1.265	0.277	1.547×10^{-4}	-1.547×10^{-4}	4.888×10^{-4}	-4.886×10^{-4}
^{187}Pb	6.393	2	2.203	1.441	1.722×10^{-4}	-1.722×10^{-4}	5.506×10^{-4}	-5.503×10^{-4}
^{189}Pb	5.915	2	3.966	3.491	2.031×10^{-4}	-2.030×10^{-4}	6.521×10^{-4}	-6.517×10^{-4}
^{191}Pb	5.402	0	4.190	5.703	2.545×10^{-4}	-2.545×10^{-4}	8.010×10^{-4}	-8.003×10^{-4}
^{187}Bi	7.779	5	−1.432	−1.844	1.193×10^{-4}	-1.193×10^{-4}	3.821×10^{-4}	-3.820×10^{-4}
^{189}Bi	7.268	5	−0.162	−0.218	1.380×10^{-4}	-1.380×10^{-4}	4.411×10^{-4}	-4.409×10^{-4}
^{191}Bi	6.780	0	1.385	0.080	1.601×10^{-4}	-1.601×10^{-4}	5.081×10^{-4}	-5.078×10^{-4}
^{193}Bi	6.307	0	3.258	1.941	1.873×10^{-4}	-1.873×10^{-4}	5.971×10^{-4}	-5.967×10^{-4}
^{195}Bi	5.832	0	5.784	4.045	2.247×10^{-4}	-2.247×10^{-4}	7.159×10^{-4}	-7.153×10^{-4}
^{209}Bi	3.137	5	26.802	25.826	9.556×10^{-4}	-9.547×10^{-4}	3.024×10^{-3}	-3.015×10^{-3}
^{211}Bi	6.750	5	2.109	1.044	2.030×10^{-4}	-2.030×10^{-4}	6.435×10^{-4}	-6.431×10^{-4}
^{213}Bi	5.988	5	5.115	4.204	2.631×10^{-4}	-2.631×10^{-4}	8.307×10^{-4}	-8.300×10^{-4}
^{187}Po	7.979	2	−2.854	−3.149	1.124×10^{-4}	-1.123×10^{-4}	3.564×10^{-4}	-3.562×10^{-4}
^{189}Po	7.694	2	−2.456	−2.304	1.266×10^{-4}	-1.266×10^{-4}	3.926×10^{-4}	-3.924×10^{-4}
^{191}Po	7.493	0	−1.658	−1.972	1.309×10^{-4}	-1.309×10^{-4}	4.178×10^{-4}	-4.176×10^{-4}
^{193}Po	7.094	0	−0.399	−0.634	1.157×10^{-4}	-1.157×10^{-4}	4.401×10^{-4}	-4.399×10^{-4}
^{195}Po	6.750	0	0.692	0.611	1.688×10^{-4}	-1.687×10^{-4}	4.978×10^{-4}	-4.975×10^{-4}
^{197}Po	6.411	0	2.079	1.952	1.903×10^{-4}	-1.903×10^{-4}	6.043×10^{-4}	-6.039×10^{-4}
^{199}Po	6.074	0	3.639	3.397	2.202×10^{-4}	-2.202×10^{-4}	6.873×10^{-4}	-6.868×10^{-4}
^{201}Po	5.799	0	4.917	4.662	2.435×10^{-4}	-2.434×10^{-4}	7.693×10^{-4}	-7.687×10^{-4}
^{203}Po	5.496	2	6.294	6.478	2.752×10^{-4}	-2.751×10^{-4}	8.735×10^{-4}	-8.727×10^{-4}
^{205}Po	5.325	0	7.193	7.101	3.008×10^{-4}	-3.008×10^{-4}	9.524×10^{-4}	-9.515×10^{-4}
^{207}Po	5.216	0	7.993	7.677	3.206×10^{-4}	-3.205×10^{-4}	1.014×10^{-3}	-1.013×10^{-3}
^{209}Po	4.979	0	9.594	9.068	3.580×10^{-4}	-3.579×10^{-4}	1.138×10^{-3}	-1.137×10^{-3}

Table 1 (continued)

Nucleus	Q_α (MeV)	l	$\lg T_{\exp}$ (s)	$\lg T_{\mathrm{cal}}$ (s)	δP^{23}	δT^{23}	δP^{24}	δT^{24}
^{211}Po	7.595	5	−0.287	−1.482	1.611×10^{-4}	-1.611×10^{-4}	5.100×10^{-4}	-5.097×10^{-4}
^{213}Po	8.536	0	−5.431	−5.597	1.301×10^{-4}	-1.301×10^{-4}	4.061×10^{-4}	-4.059×10^{-4}
^{215}Po	7.526	0	−2.749	−2.661	1.667×10^{-4}	-1.667×10^{-4}	5.276×10^{-4}	-5.273×10^{-4}
^{217}Po	6.662	0	0.196	0.409	2.161×10^{-4}	-2.161×10^{-4}	6.823×10^{-4}	-6.818×10^{-4}
^{219}Po	5.910	0	3.341	3.586	2.788×10^{-4}	-2.787×10^{-4}	8.824×10^{-4}	-8.816×10^{-4}
^{191}At	7.822	0	−2.678	−2.609	1.256×10^{-4}	-1.255×10^{-4}	3.925×10^{-4}	-3.924×10^{-4}
^{193}At	7.572	0	−1.538	−1.838	1.329×10^{-4}	-1.329×10^{-4}	4.203×10^{-4}	-4.201×10^{-4}
^{195}At	7.344	0	−0.538	−1.103	1.438×10^{-4}	-1.438×10^{-4}	4.580×10^{-4}	-4.578×10^{-4}
^{197}At	7.104	0	−0.394	−0.264	1.568×10^{-4}	-1.568×10^{-4}	4.966×10^{-4}	-4.963×10^{-4}
^{199}At	6.777	0	0.894	0.933	1.738×10^{-4}	-1.737×10^{-4}	5.513×10^{-4}	-5.510×10^{-4}
^{201}At	6.473	0	2.075	2.142	1.944×10^{-4}	-1.944×10^{-4}	6.159×10^{-4}	-6.155×10^{-4}
^{203}At	6.210	0	3.152	3.242	2.160×10^{-4}	-2.160×10^{-4}	6.829×10^{-4}	-6.825×10^{-4}
^{205}At	6.020	0	4.199	4.082	2.386×10^{-4}	-2.385×10^{-4}	7.464×10^{-4}	-7.458×10^{-4}
^{207}At	5.872	0	4.814	4.764	2.534×10^{-4}	-2.534×10^{-4}	7.999×10^{-4}	-7.992×10^{-4}
^{209}At	5.757	0	5.695	5.311	2.683×10^{-4}	-2.683×10^{-4}	8.477×10^{-4}	-8.470×10^{-4}
^{211}At	5.982	0	4.793	4.204	2.536×10^{-4}	-2.536×10^{-4}	7.995×10^{-4}	-7.989×10^{-4}
^{213}At	9.254	0	−6.903	−7.023	1.108×10^{-4}	-1.108×10^{-4}	3.474×10^{-4}	-3.473×10^{-4}
^{215}At	8.178	0	−4.432	−4.241	1.423×10^{-4}	-1.423×10^{-4}	4.496×10^{-4}	-4.494×10^{-4}
^{217}At	7.201	0	−1.487	−1.149	1.843×10^{-4}	-1.842×10^{-4}	5.817×10^{-4}	-5.814×10^{-4}
^{219}At	6.342	0	1.777	2.162	2.417×10^{-4}	-2.417×10^{-4}	7.638×10^{-4}	-7.632×10^{-4}
^{193}Rn	8.040	2	−2.939	−2.604	1.179×10^{-4}	-1.179×10^{-4}	3.802×10^{-4}	-3.801×10^{-4}
^{195}Rn	7.690	0	−2.155	−1.825	1.318×10^{-4}	-1.318×10^{-4}	4.176×10^{-4}	-4.174×10^{-4}
^{197}Rn	7.411	0	−1.268	−0.930	1.445×10^{-4}	-1.445×10^{-4}	4.554×10^{-4}	-4.552×10^{-4}
^{199}Rn	7.132	0	−0.229	0.036	1.580×10^{-4}	-1.580×10^{-4}	5.037×10^{-4}	-5.035×10^{-4}
^{203}Rn	6.630	0	1.820	1.949	1.914×10^{-4}	-1.914×10^{-4}	6.000×10^{-4}	-5.997×10^{-4}
^{205}Rn	6.387	0	2.838	2.953	2.076×10^{-4}	-2.075×10^{-4}	6.571×10^{-4}	-6.567×10^{-4}
^{207}Rn	6.251	0	3.416	3.513	2.228×10^{-4}	-2.228×10^{-4}	7.004×10^{-4}	-6.999×10^{-4}
^{209}Rn	6.155	0	4.002	3.921	2.384×10^{-4}	-2.383×10^{-4}	7.374×10^{-4}	-7.369×10^{-4}
^{211}Rn	5.966	2	5.283	5.076	2.528×10^{-4}	-2.528×10^{-4}	8.018×10^{-4}	-8.012×10^{-4}
^{213}Rn	8.245	5	−1.710	−2.670	1.391×10^{-4}	-1.391×10^{-4}	4.406×10^{-4}	-4.404×10^{-4}
^{215}Rn	8.839	0	−5.638	−5.646	1.218×10^{-4}	-1.218×10^{-4}	3.843×10^{-4}	-3.842×10^{-4}
^{217}Rn	7.887	0	−3.227	−2.970	1.542×10^{-4}	-1.542×10^{-4}	4.881×10^{-4}	-4.878×10^{-4}
^{219}Rn	6.946	2	0.598	0.467	2.025×10^{-4}	-2.025×10^{-4}	6.393×10^{-4}	-6.389×10^{-4}
^{221}Rn	6.163	2	3.844	3.696	2.605×10^{-4}	-2.604×10^{-4}	8.235×10^{-4}	-8.228×10^{-4}
^{197}Fr	7.900	0	−2.638	−2.093	1.270×10^{-4}	-1.270×10^{-4}	4.061×10^{-4}	-4.059×10^{-4}
^{199}Fr	7.817	0	−2.180	−1.848	1.333×10^{-4}	-1.333×10^{-4}	4.245×10^{-4}	-4.243×10^{-4}
^{201}Fr	7.519	0	−1.202	−0.891	1.463×10^{-4}	-1.463×10^{-4}	4.609×10^{-4}	-4.607×10^{-4}
^{203}Fr	7.275	0	−0.260	−0.040	1.589×10^{-4}	-1.589×10^{-4}	4.995×10^{-4}	-4.993×10^{-4}
^{205}Fr	7.055	0	0.597	0.736	1.717×10^{-4}	-1.716×10^{-4}	5.386×10^{-4}	-5.383×10^{-4}
^{207}Fr	6.889	0	1.192	1.349	1.820×10^{-4}	-1.820×10^{-4}	5.789×10^{-4}	-5.786×10^{-4}
^{209}Fr	6.777	0	1.752	1.769	1.908×10^{-4}	-1.907×10^{-4}	6.076×10^{-4}	-6.072×10^{-4}
^{211}Fr	6.662	0	2.328	2.207	2.053×10^{-4}	-2.052×10^{-4}	6.414×10^{-4}	-6.410×10^{-4}
^{213}Fr	6.905	0	1.536	1.226	1.929×10^{-4}	-1.929×10^{-4}	6.101×10^{-4}	-6.097×10^{-4}
^{215}Fr	9.540	0	−7.046	−6.990	1.051×10^{-4}	-1.051×10^{-4}	3.326×10^{-4}	-3.325×10^{-4}
^{217}Fr	8.469	0	−4.658	−4.284	1.330×10^{-4}	-1.329×10^{-4}	4.243×10^{-4}	-4.242×10^{-4}
^{219}Fr	7.449	0	−1.648	−1.143	1.740×10^{-4}	-1.740×10^{-4}	5.545×10^{-4}	-5.542×10^{-4}
^{221}Fr	6.458	2	2.459	2.878	2.354×10^{-4}	-2.354×10^{-4}	7.503×10^{-4}	-7.498×10^{-4}
^{223}Fr	5.561	4	7.342	7.785	3.326×10^{-4}	-3.325×10^{-4}	1.045×10^{-3}	-1.044×10^{-3}

Table 1 (continued)

Nucleus	Q_α (MeV)	l	$\lg T_{\exp}$ (s)	$\lg T_{\mathrm{cal}}$ (s)	δP^{23}	δT^{23}	δP^{24}	δT^{24}
^{201}Ra	8.002	0	−1.699	−2.035	1.297×10^{-4}	-1.297×10^{-4}	4.083×10^{-4}	-4.082×10^{-4}
^{203}Ra	7.736	0	−1.444	−1.211	1.382×10^{-4}	-1.382×10^{-4}	4.444×10^{-4}	-4.442×10^{-4}
^{205}Ra	7.486	0	−0.658	−0.389	1.551×10^{-4}	-1.551×10^{-4}	4.832×10^{-4}	-4.830×10^{-4}
^{207}Ra	7.270	2	0.205	0.661	1.651×10^{-4}	-1.650×10^{-4}	5.197×10^{-4}	-5.194×10^{-4}
^{209}Ra	7.143	0	0.673	0.815	1.724×10^{-4}	-1.724×10^{-4}	5.475×10^{-4}	-5.472×10^{-4}
^{211}Ra	7.042	0	1.100	1.187	1.820×10^{-4}	-1.820×10^{-4}	5.753×10^{-4}	-5.750×10^{-4}
^{213}Ra	6.862	2	2.274	2.137	1.943×10^{-4}	-1.943×10^{-4}	6.145×10^{-4}	-6.141×10^{-4}
^{215}Ra	8.862	5	−2.778	−3.631	9.256×10^{-5}	-9.256×10^{-5}	3.891×10^{-4}	-3.890×10^{-4}
^{217}Ra	9.161	0	−5.710	−5.727	1.132×10^{-4}	-1.132×10^{-4}	3.626×10^{-4}	-3.625×10^{-4}
^{219}Ra	8.138	2	−2.046	−2.679	1.490×10^{-4}	-1.490×10^{-4}	4.687×10^{-4}	-4.685×10^{-4}
^{221}Ra	6.880	2	1.398	1.623	2.085×10^{-4}	-2.084×10^{-4}	6.604×10^{-4}	-6.600×10^{-4}
^{223}Ra	5.979	2	5.995	5.523	2.826×10^{-4}	-2.825×10^{-4}	8.964×10^{-4}	-8.956×10^{-4}
^{205}Ac	8.090	0	−1.097	−1.930	1.309×10^{-4}	-1.309×10^{-4}	4.166×10^{-4}	-4.164×10^{-4}
^{207}Ac	7.840	0	−1.509	−1.163	1.436×10^{-4}	-1.436×10^{-4}	4.505×10^{-4}	-4.503×10^{-4}
^{209}Ac	7.730	0	−1.027	−0.801	1.481×10^{-4}	-1.481×10^{-4}	4.675×10^{-4}	-4.673×10^{-4}
^{211}Ac	7.570	0	−0.672	−0.273	1.572×10^{-4}	-1.572×10^{-4}	4.983×10^{-4}	-4.981×10^{-4}
^{213}Ac	7.498	0	−0.132	−0.050	1.644×10^{-4}	-1.644×10^{-4}	5.167×10^{-4}	-5.164×10^{-4}
^{215}Ac	7.746	0	−0.767	−0.904	1.566×10^{-4}	-1.565×10^{-4}	4.937×10^{-4}	-4.934×10^{-4}
^{217}Ac	9.832	0	−7.161	−6.961	1.267×10^{-4}	-1.267×10^{-4}	3.184×10^{-4}	-3.183×10^{-4}
^{219}Ac	8.830	0	−5.027	−4.522	1.257×10^{-4}	-1.257×10^{-4}	3.679×10^{-4}	-3.678×10^{-4}
^{221}Ac	7.790	0	−1.284	−1.461	1.630×10^{-4}	-1.630×10^{-4}	5.200×10^{-4}	-5.197×10^{-4}
^{223}Ac	6.783	2	2.105	2.440	2.204×10^{-4}	-2.204×10^{-4}	6.975×10^{-4}	-6.971×10^{-4}
^{225}Ac	5.935	2	5.933	6.226	2.927×10^{-4}	-2.926×10^{-4}	9.214×10^{-4}	-9.205×10^{-4}
^{227}Ac	5.042	0	10.696	10.970	4.093×10^{-4}	-4.092×10^{-4}	1.302×10^{-3}	-1.300×10^{-3}
^{211}Th	7.940	0	−1.319	−1.079	1.425×10^{-4}	-1.425×10^{-4}	4.544×10^{-4}	-4.542×10^{-4}
^{213}Th	7.837	0	−0.842	−0.759	1.507×10^{-4}	-1.507×10^{-4}	4.744×10^{-4}	-4.742×10^{-4}
^{215}Th	7.665	2	0.130	0.073	1.584×10^{-4}	-1.584×10^{-4}	5.044×10^{-4}	-5.042×10^{-4}
^{217}Th	9.435	5	−3.606	−4.388	1.106×10^{-4}	-1.106×10^{-4}	3.499×10^{-4}	-3.498×10^{-4}
^{219}Th	9.510	0	−5.990	−5.866	1.088×10^{-4}	-1.088×10^{-4}	3.434×10^{-4}	-3.433×10^{-4}
^{221}Th	8.625	2	−2.757	−3.324	1.348×10^{-4}	-1.347×10^{-4}	4.252×10^{-4}	-4.250×10^{-4}
^{223}Th	7.567	2	−0.222	−0.045	1.753×10^{-4}	-1.753×10^{-4}	5.552×10^{-4}	-5.549×10^{-4}
^{225}Th	6.921	2	2.766	2.321	2.130×10^{-4}	-2.129×10^{-4}	6.768×10^{-4}	-6.764×10^{-4}
^{227}Th	6.147	2	6.208	5.677	2.763×10^{-4}	-2.763×10^{-4}	8.751×10^{-4}	-8.743×10^{-4}
^{229}Th	5.168	2	11.398	10.998	4.038×10^{-4}	-4.037×10^{-4}	1.271×10^{-3}	-1.270×10^{-3}
^{211}Pa	8.480	0	−2.222	−2.347	1.267×10^{-4}	-1.267×10^{-4}	4.006×10^{-4}	-4.004×10^{-4}
^{213}Pa	8.384	0	−2.131	−2.065	1.286×10^{-4}	-1.286×10^{-4}	4.134×10^{-4}	-4.132×10^{-4}
^{215}Pa	8.240	0	−1.854	−1.643	1.382×10^{-4}	-1.381×10^{-4}	4.357×10^{-4}	-4.355×10^{-4}
^{217}Pa	8.489	0	−2.420	−2.408	1.344×10^{-4}	-1.344×10^{-4}	4.190×10^{-4}	-4.189×10^{-4}
^{219}Pa	10.130	0	−7.252	−6.935	9.647×10^{-5}	-9.646×10^{-5}	3.049×10^{-4}	-3.048×10^{-4}
^{221}Pa	9.250	0	−5.229	−4.843	1.164×10^{-4}	-1.164×10^{-4}	3.680×10^{-4}	-3.678×10^{-4}
^{223}Pa	8.340	0	−2.276	−2.378	1.468×10^{-4}	-1.468×10^{-4}	4.601×10^{-4}	-4.599×10^{-4}
^{225}Pa	7.400	2	0.233	0.962	1.889×10^{-4}	-1.889×10^{-4}	5.932×10^{-4}	-5.929×10^{-4}
^{227}Pa	6.580	0	3.431	3.914	2.411×10^{-4}	-2.410×10^{-4}	7.601×10^{-4}	-7.595×10^{-4}
^{229}Pa	5.835	1	7.432	7.548	3.082×10^{-4}	-3.081×10^{-4}	9.843×10^{-4}	-9.833×10^{-4}
^{231}Pa	5.150	0	12.013	11.367	4.109×10^{-4}	-4.107×10^{-4}	1.299×10^{-3}	-1.297×10^{-3}
^{219}U	9.950	5	−4.222	−4.935	7.225×10^{-5}	-7.225×10^{-5}	2.913×10^{-4}	-2.912×10^{-4}
^{221}U	9.890	0	−6.180	−6.063	1.066×10^{-4}	-1.066×10^{-4}	3.247×10^{-4}	-3.246×10^{-4}
^{223}U	9.158	2	−4.187	−4.030	1.219×10^{-4}	-1.219×10^{-4}	3.835×10^{-4}	-3.834×10^{-4}

Table 1 (continued)

Nucleus	Q_α (MeV)	l	$\lg T_{\exp}$ (s)	$\lg T_{\mathrm{cal}}$ (s)	δP^{23}	δT^{23}	δP^{24}	δT^{24}
^{225}U	8.007	2	−1.208	−0.696	1.608×10^{-4}	-1.607×10^{-4}	5.056×10^{-4}	-5.053×10^{-4}
^{227}U	7.235	2	1.820	1.983	1.971×10^{-4}	-1.971×10^{-4}	6.281×10^{-4}	-6.277×10^{-4}
^{229}U	6.476	0	4.239	4.842	2.534×10^{-4}	-2.533×10^{-4}	7.976×10^{-4}	-7.970×10^{-4}
^{231}U	5.576	2	9.947	9.642	3.444×10^{-4}	-3.443×10^{-4}	1.097×10^{-3}	-1.095×10^{-3}
^{233}U	4.909	0	12.701	13.505	4.623×10^{-4}	-4.621×10^{-4}	1.465×10^{-3}	-1.463×10^{-3}
^{235}U	4.678	1	16.347	15.232	5.103×10^{-4}	-5.101×10^{-4}	1.636×10^{-3}	-1.633×10^{-3}
^{219}Np	9.210	0	−3.244	−3.651	1.129×10^{-4}	-1.129×10^{-4}	3.606×10^{-4}	-3.604×10^{-4}
^{223}Np	9.650	0	−5.602	−5.160	1.064×10^{-4}	-1.063×10^{-4}	3.412×10^{-4}	-3.411×10^{-4}
^{225}Np	8.820	0	−2.187	−3.006	1.329×10^{-4}	-1.328×10^{-4}	4.176×10^{-4}	-4.174×10^{-4}
^{227}Np	7.816	3	−0.292	0.600	1.713×10^{-4}	-1.712×10^{-4}	5.426×10^{-4}	-5.423×10^{-4}
^{229}Np	7.020	1	2.547	3.092	2.127×10^{-4}	-2.126×10^{-4}	6.760×10^{-4}	-6.756×10^{-4}
^{231}Np	6.370	1	5.144	5.885	2.672×10^{-4}	-2.671×10^{-4}	8.382×10^{-4}	-8.375×10^{-4}
^{233}Np	5.630	0	8.492	9.556	3.451×10^{-4}	-3.449×10^{-4}	1.095×10^{-3}	-1.093×10^{-3}
^{235}Np	5.194	1	12.119	12.259	4.126×10^{-4}	-4.124×10^{-4}	1.320×10^{-3}	-1.318×10^{-3}
^{237}Np	4.957	1	13.830	13.809	4.684×10^{-4}	-4.682×10^{-4}	1.471×10^{-3}	-1.469×10^{-3}
^{229}Pu	7.600	2	2.258	1.501	1.819×10^{-4}	-1.819×10^{-4}	5.788×10^{-4}	-5.784×10^{-4}
^{231}Pu	6.839	0	3.582	4.195	2.273×10^{-4}	-2.273×10^{-4}	7.233×10^{-4}	-7.228×10^{-4}
^{233}Pu	6.420	2	6.001	6.277	2.655×10^{-4}	-2.654×10^{-4}	8.449×10^{-4}	-8.442×10^{-4}
^{235}Pu	5.951	0	7.723	8.325	3.143×10^{-4}	-3.142×10^{-4}	1.001×10^{-3}	-9.998×10^{-4}
^{237}Pu	5.748	1	10.968	9.484	3.477×10^{-4}	-3.476×10^{-4}	1.094×10^{-3}	-1.093×10^{-3}
^{239}Pu	5.245	0	11.881	12.371	4.235×10^{-4}	-4.233×10^{-4}	1.337×10^{-3}	-1.335×10^{-3}
^{241}Pu	5.140	2	13.265	13.300	4.450×10^{-4}	-4.448×10^{-4}	1.418×10^{-3}	-1.416×10^{-3}
^{229}Am	8.140	2	0.255	0.077	1.584×10^{-4}	-1.584×10^{-4}	5.046×10^{-4}	-5.044×10^{-4}
^{235}Am	6.576	1	5.184	5.850	2.620×10^{-4}	-2.619×10^{-4}	8.214×10^{-4}	-8.207×10^{-4}
^{239}Am	5.922	1	8.632	9.038	3.322×10^{-4}	-3.321×10^{-4}	1.042×10^{-3}	-1.041×10^{-3}
^{241}Am	5.638	1	10.135	10.600	3.708×10^{-4}	-3.707×10^{-4}	1.173×10^{-3}	-1.171×10^{-3}
^{243}Am	5.439	1	11.365	11.754	4.068×10^{-4}	-4.067×10^{-4}	1.285×10^{-3}	-1.283×10^{-3}
^{233}Cm	7.470	0	2.107	2.541	1.934×10^{-4}	-1.933×10^{-4}	6.216×10^{-4}	-6.213×10^{-4}
^{239}Cm	6.540	1	8.162	6.465	2.650×10^{-4}	-2.649×10^{-4}	8.535×10^{-4}	-8.528×10^{-4}
^{241}Cm	6.185	3	8.448	8.597	3.054×10^{-4}	-3.053×10^{-4}	9.640×10^{-4}	-9.631×10^{-4}
^{243}Cm	6.169	2	8.963	8.399	3.071×10^{-4}	-3.070×10^{-4}	9.859×10^{-4}	-9.850×10^{-4}
^{245}Cm	5.625	2	11.416	11.351	3.837×10^{-4}	-3.836×10^{-4}	1.211×10^{-3}	-1.210×10^{-3}
^{247}Cm	5.354	1	14.692	12.808	4.244×10^{-4}	-4.242×10^{-4}	1.356×10^{-3}	-1.354×10^{-3}
^{243}Bk	6.874	2	7.043	5.576	2.513×10^{-4}	-2.512×10^{-4}	7.950×10^{-4}	-7.943×10^{-4}
^{245}Bk	6.455	2	8.548	7.467	2.894×10^{-4}	-2.894×10^{-4}	9.192×10^{-4}	-9.184×10^{-4}
^{247}Bk	5.890	2	10.639	10.349	3.571×10^{-4}	-3.569×10^{-4}	1.120×10^{-3}	-1.119×10^{-3}
^{249}Bk	5.521	2	12.288	12.479	4.055×10^{-4}	-4.053×10^{-4}	1.292×10^{-3}	-1.291×10^{-3}
^{237}Cf	8.220	2	0.057	0.960	1.684×10^{-4}	-1.684×10^{-4}	5.313×10^{-4}	-5.310×10^{-4}
^{245}Cf	7.259	0	3.884	4.146	2.291×10^{-4}	-2.290×10^{-4}	7.226×10^{-4}	-7.221×10^{-4}
^{247}Cf	6.503	2	7.499	7.701	2.901×10^{-4}	-2.900×10^{-4}	9.130×10^{-4}	-9.122×10^{-4}
^{249}Cf	6.293	1	10.044	8.534	3.148×10^{-4}	-3.147×10^{-4}	9.875×10^{-4}	-9.866×10^{-4}
^{251}Cf	6.177	5	10.452	10.314	3.327×10^{-4}	-3.326×10^{-4}	1.057×10^{-3}	-1.056×10^{-3}
^{253}Cf	6.126	0	8.690	9.279	3.390×10^{-4}	-3.389×10^{-4}	1.073×10^{-3}	-1.072×10^{-3}
^{247}Es	7.464	3	3.591	4.264	2.202×10^{-4}	-2.202×10^{-4}	6.945×10^{-4}	-6.941×10^{-4}
^{251}Es	6.597	0	7.359	7.439	2.874×10^{-4}	-2.873×10^{-4}	9.085×10^{-4}	-9.077×10^{-4}
^{253}Es	6.739	0	6.248	6.759	2.825×10^{-4}	-2.824×10^{-4}	8.896×10^{-4}	-8.888×10^{-4}
^{255}Es	6.436	0	7.631	8.176	3.112×10^{-4}	-3.111×10^{-4}	9.817×10^{-4}	-9.807×10^{-4}
^{249}Fm	7.709	4	2.452	4.073	2.103×10^{-4}	-2.103×10^{-4}	6.663×10^{-4}	-6.658×10^{-4}

Table 1 (continued)

Nucleus	Q_α (MeV)	l	lgT_{exp} (s)	lgT_{cal} (s)	δP^{23}	δT^{23}	δP^{24}	δT^{24}
^{251}Fm	7.425	1	6.025	4.400	2.273×10^{-4}	-2.273×10^{-4}	7.199×10^{-4}	-7.194×10^{-4}
^{253}Fm	7.198	5	6.331	6.478	2.501×10^{-4}	-2.500×10^{-4}	7.873×10^{-4}	-7.867×10^{-4}
^{255}Fm	7.241	4	4.859	5.857	2.498×10^{-4}	-2.498×10^{-4}	7.857×10^{-4}	-7.851×10^{-4}
^{257}Fm	6.864	2	6.940	6.878	2.788×10^{-4}	-2.788×10^{-4}	8.810×10^{-4}	-8.802×10^{-4}
^{249}Md	8.441	2	1.530	1.329	1.755×10^{-4}	-1.755×10^{-4}	5.528×10^{-4}	-5.525×10^{-4}
^{251}Md	7.963	1	3.398	2.796	1.984×10^{-4}	-1.983×10^{-4}	6.276×10^{-4}	-6.273×10^{-4}
^{255}Md	7.906	2	4.358	3.122	2.084×10^{-4}	-2.084×10^{-4}	6.563×10^{-4}	-6.559×10^{-4}
^{257}Md	7.557	1	5.114	4.255	2.279×10^{-4}	-2.279×10^{-4}	7.224×10^{-4}	-7.219×10^{-4}
^{253}No	8.415	1	2.231	1.618	1.779×10^{-4}	-1.779×10^{-4}	5.680×10^{-4}	-5.677×10^{-4}
^{255}No	8.428	5	2.840	2.695	1.875×10^{-4}	-1.875×10^{-4}	5.845×10^{-4}	-5.842×10^{-4}
^{257}No	8.477	2	1.456	1.529	1.821×10^{-4}	-1.821×10^{-4}	5.771×10^{-4}	-5.768×10^{-4}
^{259}No	7.854	2	3.664	3.701	2.146×10^{-4}	-2.146×10^{-4}	6.780×10^{-4}	-6.775×10^{-4}
^{253}Lr	8.918	0	−0.154	0.324	1.604×10^{-4}	-1.604×10^{-4}	5.040×10^{-4}	-5.037×10^{-4}
^{255}Lr	8.556	0	1.494	1.464	1.768×10^{-4}	-1.767×10^{-4}	5.553×10^{-4}	-5.550×10^{-4}
^{259}Lr	8.580	0	0.899	1.333	1.789×10^{-4}	-1.789×10^{-4}	5.680×10^{-4}	-5.677×10^{-4}
^{257}Rf	9.083	5	0.748	1.368	1.648×10^{-4}	-1.647×10^{-4}	5.105×10^{-4}	-5.102×10^{-4}
^{261}Rf	8.650	0	1.057	1.483	1.798×10^{-4}	-1.798×10^{-4}	5.654×10^{-4}	-5.651×10^{-4}
^{259}Db	9.620	5	−0.292	0.147	1.463×10^{-4}	-1.463×10^{-4}	4.633×10^{-4}	-4.631×10^{-4}
^{261}Sg	9.714	2	−0.729	−0.713	1.451×10^{-4}	-1.451×10^{-4}	4.550×10^{-4}	-4.547×10^{-4}
^{261}Bh	10.500	3	−1.893	−2.201	1.239×10^{-4}	-1.239×10^{-4}	3.925×10^{-4}	-3.924×10^{-4}
^{265}Hs	10.470	0	−2.708	−2.268	1.253×10^{-4}	-1.253×10^{-4}	4.030×10^{-4}	-4.028×10^{-4}

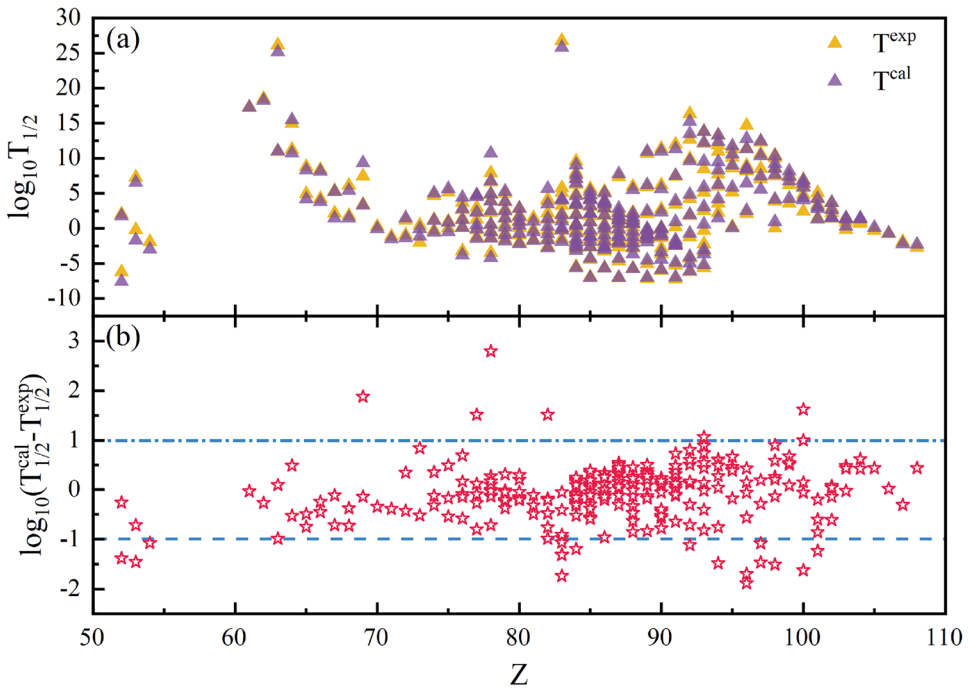

Fig. 1 (color online) Degree of concordance between theoretical half-life and experimental data. (a): The yellow and purple triangles represent the experimental data and the theoretical α-decay half-life, respectively. (b): Deviation of experimental data and the theoretical α-decay half-life

the parity of the protons they contain. The first category is for parent nuclei with an odd number of protons, also known as 'odd–even nuclei'. The second category is for parent nuclei with an even number of protons, known as 'even–odd nuclei'. In this context, we discuss the difference in the rate of change of the penetration probability of these two types of nuclei when exposed to the same laser field. Figure 2 displays the rate of change of the

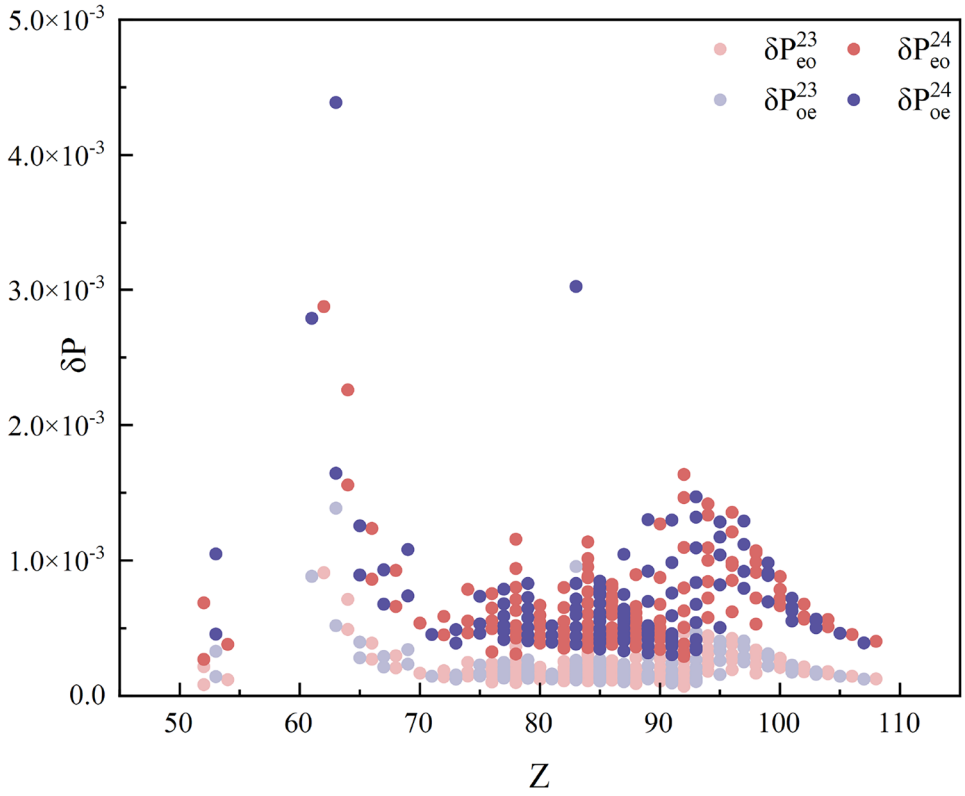

Fig. 2 (Color online) Rate of change of penetration probability for different parent nuclei for laser intensities of $I = 10^{23}$ W/cm^2 and $I = 10^{24}$ W/cm^2

penetration probability for different parent nuclei under the laser intensities of $I = 10^{23}$ W/cm^2 and $I = 10^{24}$ W/cm^2. The superscript of δP in the figure denotes the laser intensity, and the subscripts 'eo' and 'oe' of δP indicate the parent nuclei with even and odd numbers of protons, respectively.

Figure 2 illustrates that for nuclei with a smaller proton number, the rate of change of penetration probability of the even–odd nuclei is lower than that of the odd–even nuclei. This conclusion is also drawn from Table 1, where for parent nuclei with $Z \leq 70$, the mean value of δP for even–odd nuclei is 3.52×10^{-4} with a maximum of 9.1×10^{-4} in the case of $I = 10^{23}$ W/cm^2, and the mean value of δP for odd–even nuclei is 4.57×10^{-4} with a maximum of 1.39×10^{-3} in the case of $I = 10^{23}$ W/cm^2. As the number of protons increased, the rate of change in the penetration probability of the odd–even nucleus became more significant than that of the even–odd nucleus. This difference becomes more apparent as the laser intensity increases. It is observed that there are two nuclei (^{151}Eu and ^{209}Bi) with a significantly high rate of change in penetration probability. The most significant change in the penetration probability of the parent nucleus occurred in the Z range of 60–70, followed by a gradual decrease in the rate of change and a subsequent increase at $Z = 90$. This is because δP is inversely proportional to Q_α. Equation (36) in Ref. [39] gives a detailed form of the δP versus Q_α relationship. Figure 3 illustrates the distribution of δP and Q_α with Z for the odd-A nucleus, showing that values of Z in the range of 60–70, with smaller values of Q_α, result in the highest δP values. This phenomenon is also evident for the even–even kernel, where the interval of the maximum δP occurs when $60 \leq Z \leq 80$ [68]. Figure 2 also shows that the distribution of the rate of change of the penetration probability with Z for odd-A nuclei follows almost the same trend as that for even–even nuclei, showing a trend of low center and high sides [68]. In addition, the rate of change for the most laser-sensitive odd-A nucleus (^{151}Eu) was slightly higher than that for the even–even nucleus (^{144}Nd) [39]. Moreover, the rate of change for even–even nuclei is significantly higher than that for odd-A nuclei in the Z range of 70–80, which could be linked to the α decay energy [68]. Furthermore, a comparative analysis of the penetration probability rate of change for the same parent nucleus under varying laser intensities revealed that an increase in the laser intensity by an order of magnitude typically results in a tripling of the rate of change in the penetration probability. Therefore, future experiments can expect significant changes in the half-life of the nuclei as the laser intensity increases.

The α decay energy and half-life of odd-A nuclei are subject to odd–even staggering shell effects [67]. These phenomena are primarily attributed to the effect of pairwise correlations and the blocking of specific orbits by unpaired nuclei [76]. We are intrigued by the possibility that the shell effect and the odd–even staggering, which is observed in the

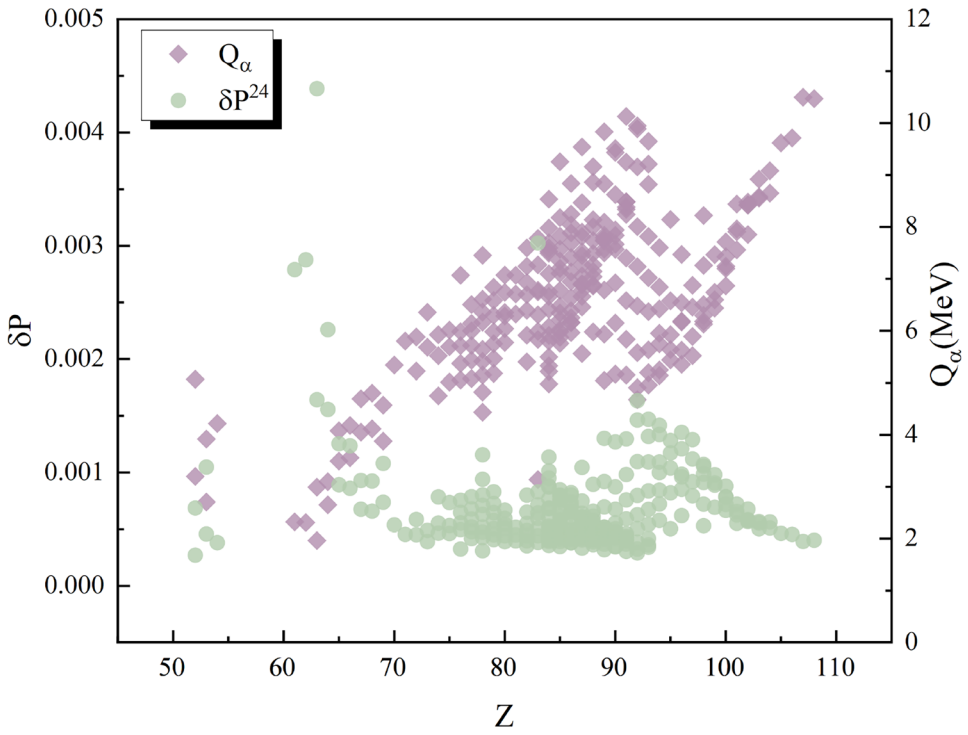

Fig. 3 (Color online) Distribution of δP and Q_α with Z for laser intensities of $I = 10^{24}$ W/cm^2

energy and half-life of odd-A nuclei, may also be reflected in the rate of change of the penetration probability in extreme laser field environments. Figures 4 and 5 depict the influence of the shell effect on δP of parent nuclei for Z values in the ranges of 80–84 and 85–90, respectively, at a laser intensity of $I = 10^{23}$ W/cm^2. Various colored circles represent different parent nuclei. These figures indicate a similar trend in δP of different parent nuclei near the neutron shell layer

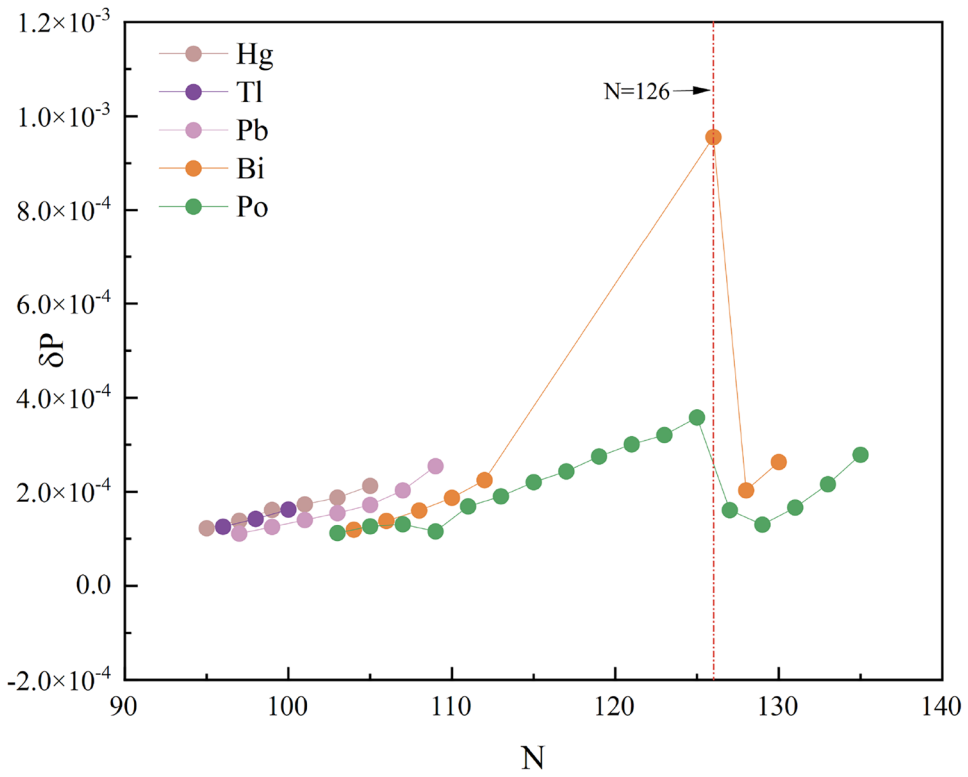

Fig. 4 (Color online) Effect of the shell effect on δP of the parent nuclei for $80 \le Z \le 84$ in the case of $I = 10^{23}$ W/cm^2

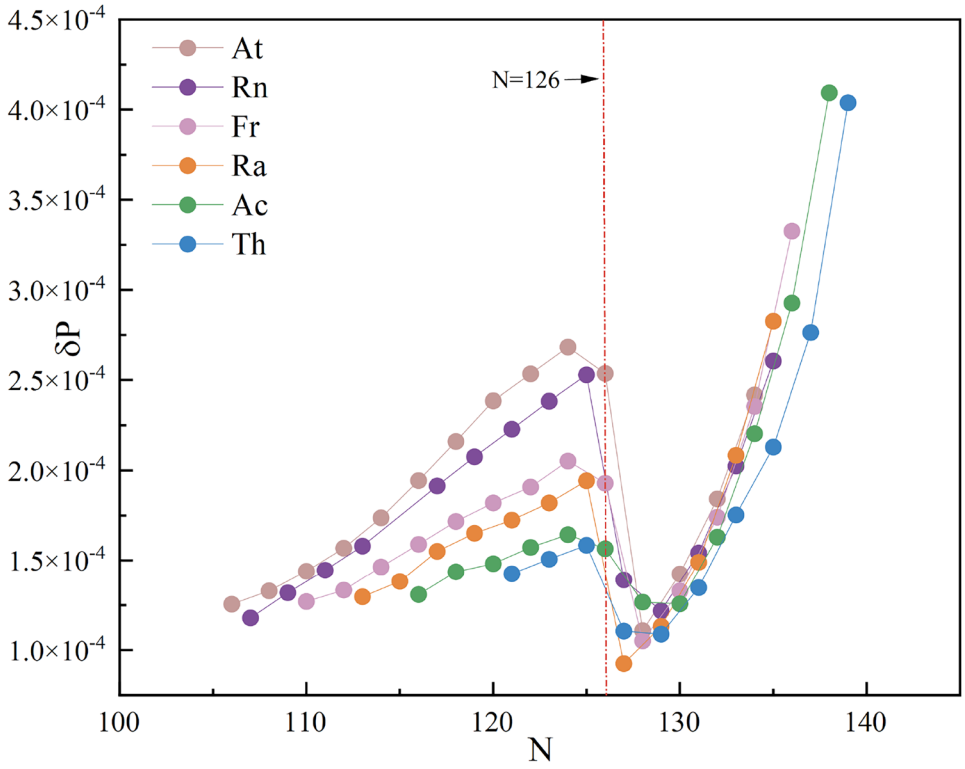

Fig. 5 (Color online) Effect of the shell effect on δP of the parent nuclei for $85 \leq Z \leq 90$ in the case of $I = 10^{23}$ W/cm^2

at 126. For parent nuclei with a neutron number of less than 126, δP increases as the neutron number increases, and then exhibits a sharp downward trend near $N = 126$. In addition, for parent nuclei with neutron numbers greater than 126, δP continued to increase as the neutron number increased. Such nuclear shell structure effects, reflected in the rate of change of the penetration probability, are caused by a mutation in the α decay energy near $N = 126$. This implies that in future experiments, it is necessary to use parent nuclei that are far away from the shell layer to obtain a more significant rate of change in the half-life.

We consider the possible nuclear structure effect on clustering to explain the relationship between the shell and α decay energy. Near $N = 126$, the shell clustering effect significantly affects the decay energy [69]. The formation probability of α particles, which is closely related to the shell clustering effect and is extracted from the experimental half-lives, shows a distinct trend near $N = 126$ [70, 71]. In nuclei with neutron numbers equal to or just below $N = 126$, such as Po, the hole character of the neutron states leads to suppression of the α formation amplitude compared to nuclei such as Po [70]. This is because in the neutron particle case (Po), high-lying configurations are more accessible, enhancing the neutron pairing correlation and eventually the two-neutron and α clustering. In contrast, in the neutron hole case, the availability of such configurations is limited, resulting in weaker clustering and a lower α formation amplitude. As the BCS theory describes, the pairing correlation is an essential factor related to the shell clustering effect. The isovector pairing correlation enhances the calculated α-decay width and governs the formation of α particles on the nuclear surface. The pairing gap, obtained from the experimental binding energies and related to the pairing correlation, showed a similar trend as the α-particle formation probability near $N = 126$ [4, 72–75]. This indicates that the pairing correlation and the resulting shell clustering effect influence the decay energy by affecting the α-particle formation probability.

Figures 6 and 7 show the odd–even staggering of the rate of change of penetration probability of parent nuclei Ra and Th in the case of $I = 10^{23}$ W/cm^2. The theoretical values of δP for the even–even nuclei used for plotting were obtained from Ref. [39]. These figures show that both parent nuclei Ra and Th exhibited odd–even staggering in the nucleus region away from the magic shell. To demonstrate this phenomenon more clearly, δP theoretical values of the parts with $N < 126$ were locally enlarged. The red circles in the magnified part represent odd-A nuclei, whereas the black circles indicate even–even nuclei. The magnified image shows an apparent parity staggering, indicating that the extent of the impact of the laser on the half-life of the nucleus is also affected by pairwise correlations and the blocking of specific orbitals by unpaired nuclei. This odd–even staggering effect is also reflected in the α-decay energy [76, 77]. Because

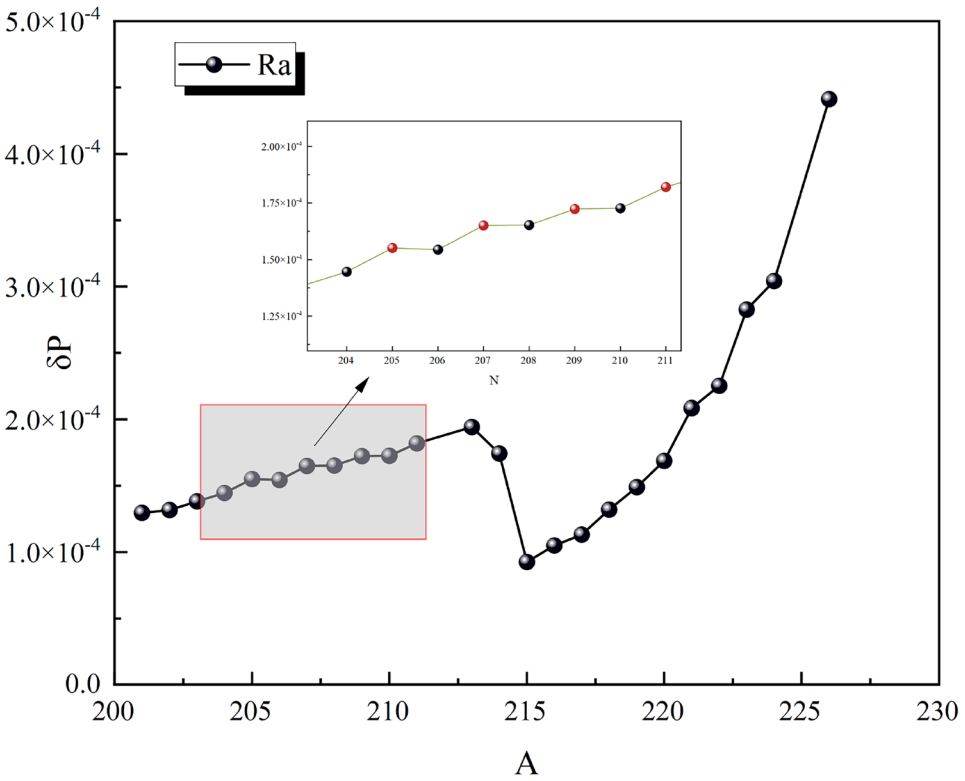

Fig. 6 (Color online) Odd–even staggering of the rate of change of penetration probability of parent nuclei Ra in the case of $I = 10^{23}$ W/cm^2

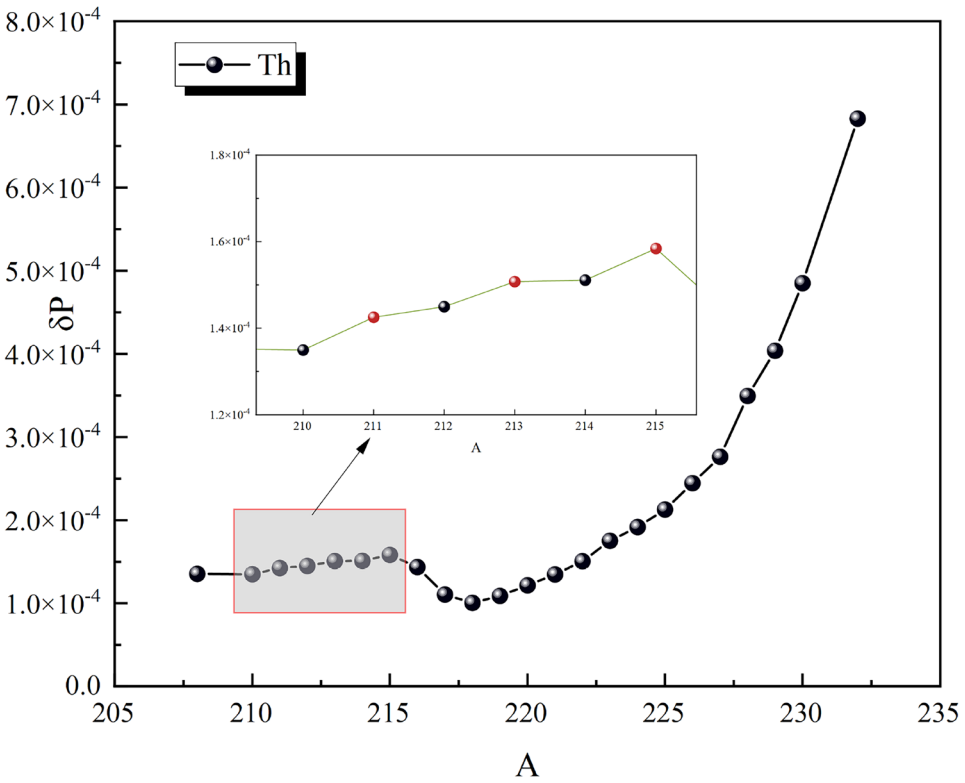

Fig. 7 (Color online) Odd–even staggering of the rate of change of penetration probability of parent nuclei Th in the case of $I = 10^{23}$ W/cm^2

the rate of change in the penetration probability is inversely proportional to the α-decay energy, the odd–even staggering effect related to the rate of change in the penetration probability tends to be opposite to the odd–even staggering effect linked to the α-decay energy.

4 Summary

We examined the effect of intense laser fields on the α-decay half-life of deformed ground-state odd-A nuclei. Our research indicated that a laser field can marginally modify the α-decay penetration probability in most nuclei, with Europium-151 (^{151}Eu) showing the most pronounced susceptibility to laser-induced alterations. Moreover, the variance in the penetration probability rate of change between even–odd and odd–even nuclei was investigated. Furthermore, the rate of change in the penetration probability of odd-A nuclei was analyzed in relation to the number of neutrons in the parent nucleus. The findings reveal that the effect of the laser field on the nucleus penetration probability is significantly influenced by both the shell effect and the odd–even staggering phenomenon.

Acknowledgements We thank Professor Xiao-Hua Li and Dr. Hai-Feng Gui for helpful discussions.

Author Contributions All authors contributed to the study conception and design. Material preparation, data collection, and analysis were performed by Jun-Hao Cheng, Tong-Pu Yu, and Qiong Xiao. The first draft of the manuscript was written by Jun-Hao Cheng, and all authors commented on previous versions of the manuscript. All authors read and approved the final manuscript.

Data Availability The data that support the findings of this study are openly available in Science Data Bank at https://cstr.cn/31253.11.sciencedb.j00186.00414 and https://doi.org/10.57760/sciencedb.j00186.00414.

Declarations

Conflict of interest The authors declare that they have no conflict of interest.

References

1. D.F. Geesaman, C.K. Gelbke, R.V.F. Janssens et al., Physics of a rare isotope accelerator. Annu. Rev. Nucl. Part. S. **56**, 53 (2006). https://doi.org/10.1146/annurev.nucl.55.090704.151604
2. S. Hofmann, G. Münzenberg, The discovery of the heaviest elements. Rev. Mod. Phys. **72**, 733 (2000). https://doi.org/10.1103/RevModPhys.72.733
3. M. Pfützner, M. Karny, L.V. Grigorenko et al., Radioactive decays at limits of nuclear stability. Rev. Mod. Phys. **84**, 567 (2012). https://doi.org/10.1103/RevModPhys.84.567
4. A.N. Andreyev, M. Huyse, P. Van Duppen et al., Signatures of the $Z = 82$ shell closure in α-decay process. Phys. Rev. Lett. **110**, 242502 (2013). https://doi.org/10.1103/PhysRevLett.110.242502
5. Z. Kalaninová, A.N. Andreyev, S. Antalic et al., α decay of the very neutron-deficient isotopes $^{197-199}$Fr. Phys. Rev. C **87**, 044335 (2013). https://doi.org/10.1103/PhysRevC.87.044335
6. L. Ma, Z.Y. Zhang, Z.G. Gan et al., α-decay properties of the new isotope ^{216}U. Phys. Rev. C **91**, 051302 (2015). https://doi.org/10.1103/PhysRevC.91.051302
7. H.B. Yang, Z.Y. Zhang, J.G. Wang et al., Alpha decay of the new isotope ^{215}U. Euro. Phys. J. A **51**, 88 (2015). https://doi.org/10.1140/epja/i2015-15088-9
8. R.J. Carroll, R.D. Page, D.T. Joss et al., Blurring the boundaries: decays of multiparticle isomers at the proton drip line. Phys. Rev. Lett. **112**, 092501 (2014). https://doi.org/10.1103/PhysRevLett.112.092501
9. S. Luo, D.M. Zhang, L.J. Qi et al., α-particle preformation factors in heavy and superheavy nuclei. Chin. Phys. C **48**, 044105 (2024). https://doi.org/10.1088/1674-1137/ad21e9
10. J.G. Deng, J.H. Cheng, X.J. Bao et al., Systematic study of cluster radioactivity within the generalized liquid drop model. Chin. Phys. C **48**, 064101 (2024). https://doi.org/10.1088/1674-1137/ad30ef
11. J.G. Deng, H.F. Zhang, Correlation between α-particle preformation factor and α decay energy. Phys. Lett. B **816**, 136247 (2021). https://doi.org/10.1016/j.physletb.2021.136247
12. Z. Wang, D. Bai, Z.Z. Ren, Improved density-dependent cluster model in α-decay calculations within anisotropic deformation-dependent surface diffuseness. Phys. Rev. C **105**, 024327 (2022). https://doi.org/10.1103/PhysRevC.91.051302
13. G. Gamow, Zur quantentheorie des atomkernes. Z. Phys. **51**, 204 (1928). https://doi.org/10.1007/BF01343196
14. R.W. Gurney, E.U. Condon, Wave mechanics and radioactive disintegration. Nature. **122**, 439 (1928). https://doi.org/10.1038/122439a0
15. A. Astier, P. Petkov, M.-G. Porquet et al., Novel manifestation of α-clustering structures: new "$\alpha + ^{208}$ Pb'' states in ^{212}Po revealed by their enhanced $E1$ decays. Phys. Rev. Lett. **104**, 042701 (2010). https://doi.org/10.1103/PhysRevLett.104.042701
16. A. Tohsaki, H. Horiuchi, P. Schuck et al., Alpha cluster condensation in ^{12}C and ^{16}O. Phys. Rev. Lett. **87**, 192501 (2001). https://doi.org/10.1103/PhysRevLett.87.192501
17. D.S. Delion, A. Sandulescu, W. Greiner, Evidence for α clustering in heavy and superheavy nuclei. Phys. Rev. C **69**, 044318 (2004). https://doi.org/10.1103/PhysRevC.69.044318
18. D. Karlgren, R.J. Liotta, R. Wyss et al., α-decay hindrance factors: a probe of mean-field wave functions. Phys. Rev. C **73**, 064304 (2006). https://doi.org/10.1103/PhysRevC.73.064304
19. Y.Q. Xin, N.N. Ma, J.G. Deng et al., Properties of $Z = 114$ superheavy nuclei. Nucl. Sci. Tech. **32**, 55 (2021). https://doi.org/10.1007/s41365-021-00899-7
20. H.C. Manjunatha, N. Sowmya, P.S. Damodara Gupta et al., Investigation of decay modes of superheavy nuclei. Nucl. Sci. Tech. **32**, 130 (2021). https://doi.org/10.1007/s41365-021-00967-y
21. N. Kinoshita, M. Paul, Y. Kashiv et al., A shorter ^{146}Sm half-life measured and implications for ^{146}Sm-^{142}Nd chronology in the solar system. Science **335**, 1614 (2012). https://doi.org/10.1126/science.1215510
22. J.W. Yoon, Y.G. Kim, I.W. Choi et al., Realization of laser intensity over 10^{23} W$/cm^2$. Optica **8**, 630 (2021). https://doi.org/10.1364/OPTICA.420520
23. Ş Mişicu, M. Rizea, Laser-assisted proton radioactivity of spherical and deformed nuclei. J. Phys. G Nucl. Part. Phys. **46**, 115106 (2019). https://doi.org/10.1088/1361-6471/ab1d7c
24. K.A. Tanaka, K.M. Spohr, D.L. Balabanski et al., Current status and highlights of the ELI-NP research program. Matter Radiat. Extrem. **5**, 024402 (2020). https://doi.org/10.1063/1.5093535
25. W.Q. Li, Z.B. Gan, L.H. Yu et al., 339 J high-energy Ti: sapphire chirped-pulse amplifier for 10 PW laser facility. Opt. Lett. **43**, 5681 (2018). https://doi.org/10.1364/OL.43.005681
26. L.P. Yu, Y. Xu, Y.Q. Liu et al., High-contrast front end based on cascaded XPWG and femtosecond OPA for 10-PW-level Ti:sapphire laser. Opt. Express **26**, 2625 (2018). https://doi.org/10.1364/OE.26.002625

27. Z.C. Li, Y. Yang, Z.W. Cao et al., Effective extraction of photoneutron cross-section distribution using gamma activation and reaction yield ratio method. Nucl. Sci. Tech. **34**, 170 (2023). https://doi.org/10.1007/s41365-023-01330-z
28. Y.R. Shou, X.Z. Wu, G.E. Ahn et al., Spatial and spectral measurement of laser-driven protons through radioactivation. Nucl. Sci. Tech. **34**, 183 (2023). https://doi.org/10.1007/s41365-023-01324-x
29. T.P. Yu, K. Liu, J. Zhao et al., Bright X/γ-ray emission and lepton pair production by strong laser fields: a review. Rev. Mod. Plasma Phys. **8**, 24 (2024). https://doi.org/10.1007/s41614-024-00158-3
30. J. Feng, W.Z. Wang, C.B. Fu et al., Femtosecond pumping of nuclear isomeric states by the coulomb collision of ions with quivering electrons. Phys. Rev. Lett. **128**, 052501 (2022). https://doi.org/10.1103/PhysRevLett.128.052501
31. Y. Shvyd'ko, R. Röhlsberger, O. Kocharovskaya et al., Resonant X-ray excitation of the nuclear clock isomer ^{45}Sc. Nature **622**, 471 (2023). https://doi.org/10.1038/s41586-023-06491-w
32. X. Wang, Substantially enhanced deuteron-triton fusion probabilities in intense low-frequency laser fields. Phys. Rev. C **102**, 011601 (2020). https://doi.org/10.1103/PhysRevC.102.011601
33. D.S. Delion, S.A. Ghinescu, Geiger-Nuttall law for nuclei in strong electromagnetic fields. Phys. Rev. Lett. **119**, 202501 (2017). https://doi.org/10.1103/PhysRevLett.119.202501
34. D.P. Kis, R. Szilvasi, Three dimensional α-tunneling in intense laser fields. J. Phys. G Nucl. Part. Phys. **45**, 045103 (2018). https://doi.org/10.1088/1361-6471/aab0d5
35. D. Bai, D.M. Deng, Z.Z. Ren, Charged particle emissions in high-frequency alternative electric fields. Nucl. Phys. A **976**, 23 (2018). https://doi.org/10.1016/j.nuclphysa.2018.05.004
36. J.T. Qi, T. Li, R.H. Xu et al., α decay in intense laser fields: calculations using realistic nuclear potentials. Phys. Rev. C **99**, 044610 (2019). https://doi.org/10.1103/PhysRevC.99.044610
37. A. Pálffy, S.V. Popruzhenko, Can extreme electromagnetic fields accelerate the α decay of nuclei? Phys. Rev. Lett. **124**, 212505 (2020). https://doi.org/10.1103/PhysRevLett.124.212505
38. Q. Xiao, J.H. Cheng, Y.Y. Xu et al., α decay in extreme laser fields within a deformed Gamow-like model. Nucl. Sci. Tech. **35**, 27 (2024). https://doi.org/10.1007/s41365-024-01371-y
39. J.H. Cheng, W.Y. Zhang, Q. Xiao et al., Determinants in laser-assisted deformed α decay. Phys. Lett. B **848**, 138322 (2024). https://doi.org/10.1016/j.physletb.2023.138322
40. D.D. Ni, Z.Z. Ren, Coupled-channels study of fine structure in the α decay of well deformed nuclei. Phys. Rev. C **83**, 067302 (2011). https://doi.org/10.1103/PhysRevC.83.067302
41. S.A. Gurvitz, G. Kalbermann, Decay width and the shift of a quasistationary state. Phys. Rev. Lett. **59**, 262 (1987). https://doi.org/10.1103/PhysRevLett.59.262
42. A. Coban, O. Bayrak, A. Soylu et al., Effect of nuclear deformation on α-decay half-lives. Phys. Rev. C **85**, 044324 (2012). https://doi.org/10.1103/PhysRevC.85.044324
43. M. Ismail, A.Y. Ellithi, M.M. Botros et al., Penetration factor in deformed potentials: application to α decay with deformed nuclei. Phys. Rev. C **86**, 044317 (2012). https://doi.org/10.1103/PhysRevC.86.044317
44. D.D. Ni, Z.Z. Ren, Systematic research on α-decay rates of spherical and deformed nuclei. Ann. Phys. **358**, 108 (2015). https://doi.org/10.1016/j.aop.2015.03.001
45. Y.B. Qian, Z.Z. Ren, D.D. Ni, Calculations of α-decay half-lives for heavy and superheavy nuclei. Phys. Rev. C **83**, 044317 (2011). https://doi.org/10.1103/PhysRevC.83.044317
46. T.L. Stewart, M.W. Kermode, D.J. Beachey et al., α-particle decay through a deformed barrier. Nucl. Phys. A **611**, 332 (1996). https://doi.org/10.1016/S0375-9474(96)00404-6
47. C. Xu, Z.Z. Ren, New deformed model of α-decay half-lives with a microscopic potential. Phys. Rev. C **73**, 041301 (2006). https://doi.org/10.1103/PhysRevC.73.041301
48. Ş Mişicu, M. Rizea, αdecay in ultraintense laser fields. J. Phys. G **40**, 095101 (2013). https://doi.org/10.1088/0954-3899/40/9/095101
49. N. Takigawa, T. Rumin, N. Ihara, Coulomb interaction between spherical and deformed nuclei. Phys. Rev. C **61**, 044607 (2000). https://doi.org/10.1103/PhysRevC.61.044607
50. M. Ismail, W.M. Seif, H. El-Gebaly, On the coulomb interaction between spherical and deformed nuclei. Phys. Lett. B **563**, 53 (2003). https://doi.org/10.1016/S0370-2693(03)00600-2
51. G.L. Zhang, X.Y. Le, Z.H. Liu, Coulomb potentials between spherical and deformed nuclei. Chin. Phys. Lett. **25**, 1247 (2008). https://doi.org/10.1088/0256-307x/25/4/023
52. J.J. Morehead, Asymptotics of radial wave equations. J. Math. Phys. **36**, 5431 (1995). https://doi.org/10.1063/1.531270
53. D.D. Ni, Z.Z. Ren, New approach for α-decay calculations of deformed nuclei. Phys. Rev. C **81**, 064318 (2010). https://doi.org/10.1103/PhysRevC.81.064318
54. K. Hagino, N. Rowley, A.T. Kruppa, A program for coupled-channel calculations with all order couplings for heavy-ion fusion reactions. Comput. Phys. Commun. **123**, 143–152 (1999). https://doi.org/10.1016/S0010-4655(99)00243-X
55. C. Xu, Z.Z. Ren, Favored α-decays of medium mass nuclei in density-dependent cluster model. Nucl. Phys. A **760**, 303 (2005). https://doi.org/10.1016/j.nuclphysa.2005.06.011
56. D. Mao, Z.W. He, Q. Gao et al., Birefringence-managed normal-dispersion fiber laser delivering energy-tunable chirp-free solitons. Ultrafast Sci. **2022**, 9760631 (2022). https://doi.org/10.34133/2022/9760631
57. J.M. Dong, W. Zuo, J.Z. Gu et al., α-decay half-lives and Q_α values of superheavy nuclei. Phys. Rev. C **81**, 064309 (2010). https://doi.org/10.1103/PhysRevC.81.064309
58. C. Xu, Z.Z. Ren, α decay of nuclei in extreme cases. Phys. Rev. C **69**, 024614 (2004). https://doi.org/10.1103/PhysRevC.69.024614
59. T. Brabec, M.Y. Ivanov, P.B.I. Corkum, Coulomb focusing on intense field atomic processes. Phys. Rev. A **54**, R2551 (1996). https://doi.org/10.1103/PhysRevA.54.R2551
60. J. Chen, J. Liu, L.B. Fu et al., Interpretation of momentum distribution of recoil ions from laser-induced nonsequential double ionization by semiclassical rescattering model. Phys. Rev. A **63**, 011404(R) (2000). https://doi.org/10.1103/PhysRevA.63.011404
61. J.T. Qi, L.B. Fu, X. Wang, Nuclear fission in intense laser fields. Phys. Rev. C **102**, 064629 (2020). https://doi.org/10.1103/PhysRevC.102.064629
62. P. Möller, A.J. Sierk, T. Ichikawa, Nuclear ground-state masses and deformations: FRDM(2012). Atom. Data Nucl. Data. **109**, 1–204 (2016). https://doi.org/10.1016/j.adt.2015.10.002
63. W.J. Huang, M. Wang, F.G. Kondev, The AME 2020 atomic mass evaluation (I). Evaluation of the input data and adjustment procedures. Chin. Phys. C **45**(3), 030002 (2021). https://doi.org/10.1088/1674-1137/abddb0
64. M. Wang, W.J. Huang, F.G. Kondev, The AME 2020 atomic mass evaluation (II). Tables, graphs, and references. Chin. Phys. C **45**, 030003 (2021). https://doi.org/10.1088/1674-1137/abddaf
65. F.G. Kondev, M. Wang, W.J. Huang, The NUBASE2020 evaluation of nuclear physics properties. Chin. Phys. C **45**, 030001 (2021). https://doi.org/10.1088/1674-1137/abddae
66. B. Buck, A.C. Merchant, S.M. Perez, New look at α decay of heavy nuclei. Phys. Rev. Lett. **65**, 2975 (1990). https://doi.org/10.1103/PhysRevLett.65.2975
67. X.D. Sun, C. Duan, J.G. Deng, Systematic study of α decay for odd-A nuclei within a two-potential approach. Phys. Rev. C **95**, 014319 (2017). https://doi.org/10.1103/PhysRevC.95.014319

68. J. H. Cheng, W. Y. Zhang, Q. Xiao *et al*., Laser-assisted deformed α decay of the ground state even-even nuclei. Preprint arXiv:2307.02095 (2023). https://doi.org/10.48550/arXiv.2307.02095
69. C. Qi, R. Liotta, R. Wyss, Recent developments in radioactive charged-particle emissions and related phenomena. Prog. Part. Nucl. Phys. **105**, 214 (2019). https://doi.org/10.1016/j.ppnp.2018.11.003
70. C. Qi, A.N. Andreyev, M. Huyse, Abrupt changes in α-decay systematics as a manifestation of collective nuclear modes. Phys. Rev. C **81**, 064319 (2010). https://doi.org/10.1103/PhysRevC.81.064319
71. C. Qi, R. Liotta, R. Wyss, Nuclear clustering and generalization of the Geiger-Nuttall law 100 years after its formulation. J. Phys. Conf. Ser. **321**, 012048 (2011). https://doi.org/10.1088/1742-6596/321/1/012048
72. S.A. Changizi, C. Qi, R. Wyss, Empirical pairing gaps, shell effects, and di-neutron spatial correlation in neutron-rich nuclei. Nucl. Phys. A **940**, 210 (2015). https://doi.org/10.1016/j.nuclphysa.2015.04.010
73. W. Satuła, J. Dobaczewski, W. Nazarewicz, Odd-even staggering of nuclear masses: pairing or shape effect? Phys. Rev. Lett. **81**, 3599 (1998). https://doi.org/10.1103/PhysRevLett.81.3599
74. C. Qi, S.A. Changizi, Density dependence of the pairing interaction and pairing correlation in unstable nuclei. Phys. Rev. C **91**, 024305 (2015). https://doi.org/10.1103/PhysRevC.91.024305
75. C. Qi, Double binding energy differences: mean-field or pairing effect? Phys. Lett. B **717**, 436–440 (2012). https://doi.org/10.1016/j.physletb.2012.10.011
76. H.B. Yang, Z.G. Gan, Z.Y. Zhang et al., New isotope ^{207}Th and odd-even staggering in α-decay energies for nuclei with $Z > 82$ and $N < 126$. Phys. Rev. C **105**, L051302 (2022). https://doi.org/10.1103/PhysRevC.105.L051302
77. H.B. Yang, Z.G. Gan, Z.Y. Zhang, Examining the impact of α -decay energies on the odd-even staggering in half-lives: α -decay spectroscopy of $^{207-209}$Ac. Phys. Rev. C **106**, 064311 (2022). https://doi.org/10.1103/PhysRevC.106.064311